Kinetic description of plasmas produced in multiphoton-ionization processes

C. Altucci, R. Bruzzese, C. de Lisio, and S. Solimeno
Dipartimento di Scienze Fisiche, Università di Napoli "Federico II", 80125 Napoli, Italy
(Received 3 February 1992; revised manuscript received 21 October 1993)

A kinetic description of inhomogeneous plasmas produced by irradiating an atomic gas by a well-focused ultrashort high-intensity laser pulse is presented. The Vlasov-Maxwell equation is integrated by representing the distribution function $f(\mathbf{r},\mathbf{v};t)$ in the form $f_0(D\mathbf{r}-B\mathbf{v},-C\mathbf{r}+A\mathbf{v})$, with f_0 the initial distribution and the A,B,C,D functions depending on $\mathbf{r}$, $\mathbf{v}$, and t. On the basis of this representation the evolution of some charge distributions is examined, by focusing the attention on the transport of ion packets, the effect of the ponderomotive potential, and the capture of electrons by the ion potential well.

PACS number(s): 52.25.Dg, 52.25.Wz, 32.80.Wr

I. INTRODUCTION

Focusing ultrashort light pulses on a gas jet emerging from a needle injector inside an evacuated scattering chamber, the atoms ionize thus producing a plasma of small dimension and low density. In nonresonant multiphoton ionization (MPI) processes a plasma is created in a very short time (100 fsec–100 psec) in a region of 10–40 μm, while energetic electrons blast off, heading through the scattering chamber [1]. When very intense ultrashort laser pulses are used in nonresonant MPI processes, the electron energy spectrum consists of some peaks approximately spaced by the photon energy [Above-Threshold Ionization (ATI)]. The ions are separated from the electrons by means of an extraction field and reach their end by hitting a detector placed beside the ionization chamber, after being accelerated by a uniform electric field. The ion detector signal is the result of a very complex process beginning in a small region where the laser pulse interacts with the gas and ending at the detector after a flight through acceleration and drift regions. Figure 1 illustrates schematically the situation showing a typical experimental setup.

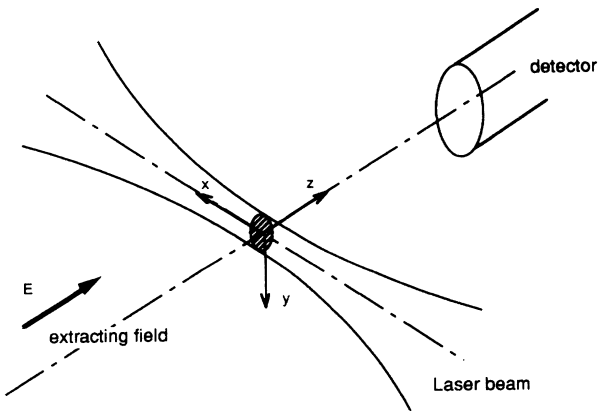

FIG. 1. Typical MPI setup. The electric field in proximity of the laser focus is used for separating the ions from the electrons.

In most MPI experiments the gas pressure and the time of observation are so small to allow a perturbative account of the electron-electron and electron-ion collisions. An important exception to these conditions occurs in the harmonic generation, where the pressure is so high that collision effects cannot be ignored [2].

Two levels of theoretical description are available [3, 4] for a collisionless nonneutral plasma: (a) macroscopic fluid description based on the moment-Maxwell equations, (b) kinetic description based either on particle simulation or on the integration of Vlasov-Maxwell equation.

In the macroscopic fluid description the time development of the macroscopic properties of the plasma, such as number density, mean velocity, and pressure tensor are examined. These quantities evolve in terms of the electric field determined from Poisson's equation. If the plasma is cold, variations in the pressure can be ignored and this approximation results in a closed description of the time development of the number density, mean velocity, and electric field. The fluid description was adopted in Ref. [5] for analyzing the evolution of packets in presence of electric fields varying linearly in space. The analysis was restricted to Gaussian space distributions of the plasma constituents and depended heavily on numerical solutions.

The particle-simulation approach [6, 7] has been used in various forms for analyzing the evolution of inhomogeneous and non-Maxwellian plasmas in presence of inhomogeneous electric field.

An alternative to simulations using particles is the integration of the collisionless kinetic equation, which treats phase space as a continuum. The direct integration of the Vlasov-Maxwell equation is generally less frequently adopted due to mathematical difficulties [7]. Fortunately, these difficulties reduce notably for MPI plasmas, as it will be shown in the following.

Due to the negligible values of the electron-electron and electron-ion collision frequencies for the charge densities typical of these experiments ($P \leq 10^{-4}$ Torr), discrete particle interactions may be omitted from the analysis, and collective processes can be assumed to dominate

on the time and length scales of interest. Accordingly, the particle distribution evolutions may be described by means of Vlasov equation, with electric fields consistent with the space-charge densities and static fields present in time-of-flight (TOF) spectrometers. In addition, it happens that the plasma evolves under the dominant action of its space-charge field for a time interval relatively short. This circumstance legitimatizes some important mathematical simplifications in the integration of the Vlasov equation, which will be documented in this paper.

The kinetic equations have been integrated by using the initial distribution functions f_0 of the electrons and ions. The distribution function $f(\mathbf{r},\mathbf{v};t)$ has been represented in the form $f_0(D\mathbf{r}-B\mathbf{v},-C\mathbf{r}+A\mathbf{v})$ where A,B,C, and D are functions of $\mathbf{r},\mathbf{v}$, and time t, whose equations of motion have been derived from the Vlasov equation. These equations contain the parameter $\omega^2(\mathbf{r},t)\propto qE(\mathbf{r},t)/mr$, E being the electric field acting on the plasma, q and m the charge and mass, respectively. For analyzing the expansion of a charged packet we found convenient to expand A,B,C, and D in power series in the velocity v. We found that the number of terms of the series depends on the value of the phase $\phi=\int_0^\tau \omega dt$, τ being the characteristic expansion time. Using the parameters ω and τ of typical MPI experiments we found that the series reduces to the zeroth order term for $\phi\leq 1$. Typical ion densities are about 10^{12} cm^{-3}, and in experiments on Xe, ω is about 10^8 sec^{-1} for the ions, while τ is of the order of 10 nsec, so that $\phi\approx 1$ and the series expansion can be truncated to the zeroth order.

In our analysis we found it useful to express t as a fraction of the characteristic time τ needed by a test particle for spanning the charge packet when moving with the effective velocity of the distribution. Analogously, we found it convenient to discuss the influence of space-charge effects by introducing the ratio $\mathcal{U}$ of the electric and thermal energies of the packet.

We have illustrated the above method of integration by addressing two problems encountered in MPI ionization. The first subject to be discussed, already analyzed by several authors (see for example Ref. [8]) is the dependence of the ion yield on laser properties. The total ion yield has been obtained from an integration over space and time that involves the laser intensity. In particular, the finite acceptance of the particle detector has been accounted by introducing a limit on the volume of integration [8]. In order to represent the experimental conditions more accurately, we have followed the charged cloud during the flight toward the detector. Integrating a differential system using as input the initial distribution and the potential profile along the axis of the TOF spectrometer, the detector signal has been calculated. The accuracy of this simulation has been tested against some signals measured in well-controlled experimental conditions, typical of nonresonant MPI experiments. The calculation has been carried out by disregarding the interaction between the ion and electron packets. This is a reasonable approximation in nonresonant MPI, where most of the electrons (in fact almost 100%) are produced as energetic ATI electrons and, thus, able to leave immediately the interaction volume, where the thermal ions can be considered as frozen.

The second problem discussed is connected with the interaction of the electrons with the ponderomotive potential [9] and the trapping of some of them by the potential well created by the ions.

The paper is organized in ten sections. Section II is dedicated to the discussion of the Vlasov equation for the electrons and ions interacting with a static external electric field. For getting rid of the accelerations introduced by the axial component of the external field, two moving reference frames traveling, respectively, with the centers O_e,O_i of the electron and ion distributions, have been introduced. The integration of the Vlasov equations is carried out in Sec. III by introducing the functions A,B,C, and D. The expansion of A,B,C, and D with respect to the velocity is discussed in Sec. IV and applied to Gaussian and uniform distributions in Sec. V. In Sec. VI the error deriving from the field linear profile approximation is minimized by using a variational approach. Section VII is dedicated to the expansion of some typical distributions. In particular, the charge transport through an electrostatic spectrometer is examined in Sec. VIII and compared with the signals measured in well-controlled conditions. Section IX is dedicated to the expansion of the electron packet and to the effects of the ponderomotive potential. Finally, the trapping of the electrons by the ion potential well is discussed in Sec. X. The effects of the collisions on the plasma oscillations are discussed in the framework of Hubbard-Thompson random field approximation.

II. MEAN FIELD THEORY

Let us consider two packets of electrons and ions with centers in $\mathbf{R}_e(t)$ and $\mathbf{R}_i(t)$, produced by multiphoton ionization in the waist of a laser beam focused to a spot of some microns. We analyze the evolution of the system by introducing the distribution functions $f_e(\mathbf{r},\mathbf{v},t)$ and $f_i(\mathbf{r},\mathbf{v},t)$ for electrons and ions, respectively, measuring the number densities of particles in the respective phase spaces. The evolution of these distributions is described by the Vlasov equation [3]

$$\frac{D}{Dt}f\equiv\left(\frac{\partial}{\partial t}+\mathcal{L}\right)f=0, \tag{1}$$

where

$$\mathcal{L}_e=\mathbf{v}\cdot\nabla-\frac{e}{m_e}(\mathbf{E}^{(\mathrm{sc})}+\mathbf{E}^{(\mathrm{ext})}+\mathbf{E}^{(\mathrm{pon})})\cdot\nabla_v, \tag{2a}$$

$$\mathcal{L}_i=\mathbf{v}\cdot\nabla+\frac{e}{m_i}(\mathbf{E}^{(\mathrm{sc})}+\mathbf{E}^{(\mathrm{ext})})\cdot\nabla_v \tag{2b}$$

with $e>0$. $\mathbf{E}^{(\mathrm{ext})}$ represents the external field used for extracting, focusing, and directing the electrons and ions toward the end of a TOF spectrometer. For an electrostatic TOF, $\mathbf{E}^{(\mathrm{ext})}$ corresponds to an electric potential rotationally symmetric around the flight direction. $\mathbf{E}^{(\mathrm{sc})}$ represents the coarse-grained electric field generated by the ion and electron clouds, while $-e\mathbf{E}^{(\mathrm{pon})}=-\nabla V^{(\mathrm{pon})}$ stands for the force associated to the ponderomotive potential [9]

$$V^{(\mathrm{pon})}(\mathbf{r},t)=\frac{e^2E^{(\mathrm{las})2}(\mathbf{r},t)}{4m_e\omega^{(\mathrm{las})2}}, \tag{3}$$

$\mathbf{E}^{(\mathrm{las})}$ and $\omega^{(\mathrm{las})}$ being, respectively, the electric field and the frequency of the laser beam. Accordingly, expressing $\mathrm{E}^{(\mathrm{las})}$ by means of the intensity $I^{(\mathrm{las})}(\mathbf{r},t)$,

$$\mathbf{E}^{(\mathrm{pon})}(\mathbf{r},t)=\frac{2\pi e}{c\,m_e\omega^{(\mathrm{las})2}}\nabla I(\mathbf{r},t), \tag{4}$$

where Gaussian units have been used.

As pointed out by Jonsson [9] the expression (3) of the ponderomotive potential rests on a classical description of the electron in the laser field, which becomes more reliable with increasing intensity.

We have neglected in (2) the Lorentz force term, having limited our analysis to systems not using magnetic fields for increasing the aperture of the electron spectrometer, as done, for example, in the magnetic bottle developed by Kruit and Read [10].

The penalty paid for this representation of the Coulomb interactions among the single particles is the loss of information about the particle correlation. On the other hand, for plasmas produced in MPI processes occurring at low pressures ($P\leq 10^{-4}$ Torr) the electron-electron and electron-ion collision frequencies are much smaller than the typical inverse duration of the detection process. Consequently, the plasma evolution is well described by a Vlasov equation with a self-consistent mean field, which satisfies the Poisson equation relative to the space-charge distribution. In Sec. X we will remove this assumption by including in Eq. (2a) a weak random field representing collision effects.

During their evolutions we can distinguish in each cloud a core clustered about a center of gravity (O_e,O_i). The external field tries to extract particles from these clouds; as a result, the clouds appear to lose particles during their lifetime. Consequently, we can imagine the whole MPI process as the flight of two clusters which change size, shape, and number of particles while flying toward the opposite ends of the detection apparatus. In turn, we can separate the motion of the center of gravity of each cluster from the variation of its shape and particle number. For example, it is important to imagine what remains of the ion cloud after the interaction with the electrons in the region of formation of the plasma, traveling with accelerated motion down the time-of-flight pipe while undergoing some expansion about its center of gravity due to the thermal fluctuations and the Coulomb repulsion. The separation in two centers of gravity suggested by this example proves particularly useful for getting rid of, in a very simple way, the effects due to the external field.

As a preliminary point, we notice that the distribution functions and the relative number densities are the same in the laboratory frame and in the frames with centers in O_e and O_i, respectively, namely $f(\mathbf{r},\mathbf{v},t)=f'(\mathbf{r}',\mathbf{v}',t)$, $\rho(\mathbf{r},t)=\rho'(\mathbf{r}',t)$, where primed and unprimed quantities refer to the two systems, respectively.

Next, let us introduce two transformations connecting the laboratory frame to the frames O_e and O_i, with origins in $\mathbf{R}_e(t)$ and $\mathbf{R}_i(t)$, respectively, and translating with instantaneous velocities $\mathbf{V}_e=d\mathbf{R}_e/dt$ and $\mathbf{V}_i=d\mathbf{R}_i/dt$,

$$\begin{aligned}&\mathbf{r}'_e\equiv\mathbf{r}_e-\mathbf{R}_e(t),\qquad \mathbf{v}'_e\equiv\mathbf{v}_e-\mathbf{V}_e(t),\\&\mathbf{r}'_i\equiv\mathbf{r}_i-\mathbf{R}_i(t),\qquad \mathbf{v}'_i\equiv\mathbf{v}_i-\mathbf{V}_i(t),\end{aligned} \tag{5}$$

where $\mathbf{r}'$ and $\mathbf{v}'$ are the position vectors and the velocities in O_e and O_i, respectively.

The distribution function $f'_e(\mathbf{r}'_e,\mathbf{v}'_e,t)$ of the electrons in O_e satisfies the Vlasov-Maxwell equation (1) with $\mathcal{L}_e$ replaced by

$$\mathcal{L}'_e\equiv\mathbf{v}'_e\cdot\boldsymbol{\nabla}'-\left(\frac{1}{m_e}\mathbf{F}'_e+\frac{d}{dt}\mathbf{V}_e\right)\cdot\nabla_{v'_e}. \tag{6}$$

$\mathbf{F}'_e$ representing the Lorentz force [11] in O_e,

$$\mathbf{F}'_e=e\left(\gamma_e+\frac{1-\gamma_e}{V_e^2}\mathbf{V}_e\mathbf{V}_e\right)\cdot\mathbf{E}_e-e\frac{\gamma_e}{c^2}\mathbf{v}'_e\times(\mathbf{V}_e\times\mathbf{E}_e), \tag{7}$$

where $\gamma_e=(1-\dot{R}_e^2/c^2)^{-1/2}$. For electrons with energies less than 1 keV, Eq. (7) shows that $\mathbf{F}'_e/e$ coincides with $\mathbf{E}_e$ to within an accuracy of 10^{-3}. Similar conclusions hold true for the ions. Hence, in the following we will assume $\mathbf{F}'_{e,i}/e$ coincident with the electric field in the laboratory frame, so that

$$\begin{aligned}\mathcal{L}'_e&=\mathbf{v}'_e\cdot\boldsymbol{\nabla}'-\frac{e}{m_e}\mathbf{E}'_e\cdot\nabla_{v'_e},\\\mathcal{L}'_i&=\mathbf{v}'_i\cdot\boldsymbol{\nabla}'+\frac{e}{m_i}\mathbf{E}'_i\cdot\nabla_{v'_i},\end{aligned} \tag{8}$$

where

$$\begin{aligned}\mathbf{E}'_e(\mathbf{r}'_e,t)&=\mathbf{E}^{(\mathrm{ext})}(\mathbf{r}'_e+\mathbf{R}_e)+\mathbf{E}^{(\mathrm{pon})}(\mathbf{r}'_e+\mathbf{R}_e)\\&\quad+\mathbf{E}^{(i)}(\mathbf{r}'_e-\boldsymbol{\Delta},t)+\mathbf{E}^{(e)}(\mathbf{r}'_e,t)+\frac{m_e}{e}\mathbf{A}_e,\\\mathbf{E}'_i(\mathbf{r}'_i,t)&=\mathbf{E}^{(\mathrm{ext})}(\mathbf{r}'_i+\mathbf{R}_i)\\&\quad+\mathbf{E}^{(e)}(\mathbf{r}'_i+\boldsymbol{\Delta},t)+\mathbf{E}^{(i)}(\mathbf{r}'_i,t)-\frac{m_i}{e}\mathbf{A}_i\end{aligned} \tag{9}$$

being $\boldsymbol{\Delta}=\mathbf{R}_i-\mathbf{R}_e$, while $\mathbf{A}_e=d\mathbf{V}_e/dt$ and $\mathbf{A}_i=d\mathbf{V}_i/dt$ are the accelerations. $\mathbf{E}^{(i)}$ and $\mathbf{E}^{(e)}$ represent the mean fields generated by the ion and electron clouds, respectively. The arguments of $\mathbf{E}^{(e)}$ and $\mathbf{E}^{(i)}$ are the radius vectors with origins in O_e and O_i, respectively.

The centers $\mathbf{R}_e=Z_e\hat{z}$ and $\mathbf{R}_i=Z_i\hat{z}$ of O_e and O_i move along the z axis (TOF axis), with accelerations, respectively, equal to

$$\begin{aligned}\mathbf{A}_e&=-\frac{e}{m_e}[\mathbf{E}^{(\mathrm{ext})}(\mathbf{R}_e)+\mathbf{E}^{(i)}(-\boldsymbol{\Delta},t)],\\\mathbf{A}_i&=\frac{e}{m_i}[\mathbf{E}^{(\mathrm{ext})}(\mathbf{R}_i)+\mathbf{E}^{(e)}(\boldsymbol{\Delta},t)].\end{aligned} \tag{10}$$

Since the ion cloud is small on the scale of variation of $\mathbf{E}^{(\mathrm{ext})}$, we can expand the latter one in the form

$$\mathbf{E}^{(\mathrm{ext})}(\mathbf{r}'_i+\mathbf{R}_i)=\mathbf{E}^{(\mathrm{ext})}(\mathbf{R}_i)-V_0''(Z_i)\left(z'_i\hat{z}-\frac{x'_i}{2}\hat{x}-\frac{y'_i}{2}\hat{y}\right). \tag{11}$$

V_0 being the external electric potential along the z axis. Combining (11) with (10) and substituting into (9) finally yields,

$$\mathbf{E}'_e = \mathbf{E}^{(\mathrm{pon})}(\mathbf{R}_e + \mathbf{r}'_e, t) + \mathbf{E}^{(i)}(\mathbf{r}'_e - \boldsymbol{\Delta}, t) + \mathbf{E}^{(e)}(\mathbf{r}'_e, t) - \mathbf{E}^{(i)}(-\boldsymbol{\Delta}, t), \tag{12a}$$

$$\mathbf{E}'_i = -V''_0(Z_i)\left(z'_i\hat{z} - \tfrac{1}{2}x'_i\hat{x} - \tfrac{1}{2}y'_i\hat{y}\right) + \mathbf{E}^{(i)}(\mathbf{r}'_i, t) + \mathbf{E}^{(i)}(\mathbf{r}'_i + \boldsymbol{\Delta}, t) - \mathbf{E}^{(e)}(\boldsymbol{\Delta}, t). \tag{12b}$$

Notice that we have omitted the term proportional to V''_0 from (12a) since in MPI experiments no focusing electrostatic field is generally used for the electrons. Analogously, we have omitted the ponderomotive force from the ion field due to its small incidence on the ion dynamics.

As already mentioned in the Introduction, we shall investigate in the next six sections the problem of the expansion of single charged packets (in particular ions), in the hypothesis of a linear space-charge field profile and neglecting the interaction between electron and ion packets. This kind of approach to the problem is justified since our analysis is aimed to investigate the conditions typical of nonresonant MPI processes, where the use of high intensity laser radiation ($I \geq 10^{12}$ W/cm^2) leads essentially to the production of energetic ATI electrons (with kinetic energies in excess of 1 eV) that can leave the plasma during the process of ionization or immediately after it, while the thermal ions can be considered as frozen in the interaction volume.

The problem of the interaction between ion and electron packets will be analyzed briefly and in a simplified way in Sec. X with reference to resonance MPI experiments where use is made of low intensity laser sources ($I \leq 10^9$ W/cm^2) and a higher number of thermal electrons is normally produced.

III. INTEGRATION OF THE VLASOV EQUATION

Let us consider a one-dimensional plasma and write the total derivative D/Dt of the Vlasov equation as

$$\frac{D}{Dt} = \frac{\partial}{\partial t} + v\frac{\partial}{\partial \xi} + \omega^2(\xi, t)\xi\frac{\partial}{\partial v}, \tag{13}$$

where $\omega^2(\xi, t) = qE(\xi, t)/m\xi$ with $q = e$ and $-e$ for ions and electrons, respectively. A negative ω^2 corresponds to a force directed toward the center $\xi = 0$.

Having considered a collisionless plasma, we can represent the distribution function at time t in the form

$$f(\xi, v; t) = f_0(\xi_0, v_0) \tag{14}$$

with f_0 the distribution function at $t = 0$ and

$$v_0 = v_0(\xi, v, t) = v - \int_0^t \xi(t')\omega^2[\xi(t'), t']dt',$$

$$\xi_0 = \xi_0(\xi, v, t) = \xi - vt + \int_0^t dt' \int_0^{t'} \xi(t'')\omega^2[\xi(t''), t']dt''. \tag{15}$$

According to (14) and (15), for calculating $f(\xi, v; t)$ we must integrate the equation of motion for a representative set of particles present in the plasma.

Here we want to discuss a procedure based on the representation of ξ_0 and v_0 in the form

$$\xi_0 = D(\xi, v, t)\xi - B(\xi, v, t)v, \tag{16a}$$

$$v_0 = -C(\xi, v, t)\xi + A(\xi, v, t)v \tag{16b}$$

with A, B, C, and D functions of ξ, v, and t. Plugging (16) into (14) we immediately see that Eq. (1) is satisfied by imposing

$$\frac{D}{Dt}A = C, \tag{17a}$$

$$\frac{D}{Dt}B = D, \tag{17b}$$

$$\frac{D}{Dt}C = \omega^2 A, \tag{17c}$$

$$\frac{D}{Dt}D = \omega^2 B, \tag{17d}$$

together with the initial conditions $A(\xi, v; 0) = D(\xi, v; 0) = 1$, $B(\xi, v; 0) = C(\xi, v; 0) = 0$.

The quantities A, B, C, and D can be considered as the elements of a matrix

$$\mathbf{T} = \begin{pmatrix} A & B \\ C & D \end{pmatrix} \tag{18}$$

representing a transformation in the $\xi - v$ phase plane of the initial vector $\mathbf{X}_0$ into $\mathbf{X} = \mathbf{T} \cdot \mathbf{X}_0$. Then, Eq. (14) can be recast as

$$f(\mathbf{X}, t) = f_0(\mathbf{T}^{-1} \cdot \mathbf{X}) = f_0(\mathbf{X}_0). \tag{19}$$

Equation (17) implies $(D/Dt)\ \det(\mathbf{T}) = 0$. Then, in view of the initial conditions, $\det(\mathbf{T})=1$ along the orbit of a test particle, a relation reminiscent of the property of the Boltzmann equation of preserving the total number of particles.

The system (17) can be recast as

$$\frac{D}{Dt}\mathbf{T} = \begin{pmatrix} 0 & 1 \\ \omega^2 & 0 \end{pmatrix} \cdot \mathbf{T} \equiv \mathbf{L} \cdot \mathbf{T} \tag{20}$$

where $\mathbf{L}$ is a matrix depending on the coordinate of the test particle.

Further, differentiating (20) with respect to time yields

$$\frac{D^2}{Dt^2}\mathbf{T} - \omega^2\mathbf{T} = \frac{D\omega^2}{Dt}\begin{pmatrix} 0 & 0 \\ 1 & 0 \end{pmatrix} \cdot \mathbf{T}. \tag{21}$$

In particular,

$$\frac{D^2}{Dt^2}A - \omega^2 A = 0,$$

$$\frac{D^2}{Dt^2}B - \omega^2 B = 0. \tag{22}$$

Combining (16a) with (17b) and (16b) with (17a) yields $(D/Dt)(B/\xi) = \xi_0/\xi^2$ and $(D/Dt)(A/\xi) = -v_0/\xi^2$, so that

$$B(\xi,v,t)=\xi\xi_0\int_0^t\frac{dt'}{\xi^2(\xi_0,v_0,t')},$$
$$A(\xi,v,t)=-\frac{v_0}{\xi_0}B(\xi,v,t)+\frac{\xi}{\xi_0}. \tag{23}$$

These relations explain the link between the particle trajectories $\xi(t)=\xi(\xi_0,v_0,t)$ and the $\mathbf{T}$ matrix. The choice between a description based either on trajectories or on $\mathbf{T}$ is just a matter of mathematical convenience. It will become clear in the following that $\mathbf{T}$ helps notably in finding approximate solutions for MPI plasmas.

When the space-charge field is created by the 1D charge distribution f, then

$$\omega^2(\xi,t)=\frac{e^2}{2\epsilon_0 m}\frac{1}{\xi}\left[\int_{-\infty}^{\xi}\rho(x,t)dx-\int_{\xi}^{\infty}\rho(x,t)dx\right] \tag{24}$$

with ρ the particle number density

$$\rho(\xi,t)=\int_{-\infty}^{\infty}f_0[\,D(\xi,v,t)\xi-B(\xi,v,t)v,-C(\xi,v,t)\xi+A(\xi,v,t)v]dv. \tag{25}$$

For a charge distribution symmetric with respect to the origin $\xi=0$, ω^2 reduces to

$$\omega^2(\xi,t)=\Omega^2(t)\frac{1}{\xi}\int_0^{\xi}\frac{\rho(x,t)}{\rho(0,t)}dx \tag{26}$$

with

$$\Omega^2(t)=\frac{e^2\rho(0,t)}{\epsilon_0 m}. \tag{27}$$

For typical MPI plasmas ω is almost constant in the region occupied by the particles and decays smoothly outside.

For integrating the differential system (17) it will be necessary to calculate at each step the matrix $\mathbf{T}$ and the function ω. In general, the integration of (17) is a quite difficult task, which can be accomplished by making some suitable approximations. In particular, when ω is independent of ξ the matrix $\mathbf{T}$ is independent of ξ and v and (17) reduces to an ordinary differential system in t. Similarly, when ω is approximated by a piecewise function of ξ, $\mathbf{T}$ can be expressed as a suitable combination of matrices, each of them containing elements depending only on time. In other cases it will be necessary to expand the elements of $\mathbf{T}$ in power series in the velocity and truncate the series at some order. All these approximations will be discussed in the following.

A. 3D distributions

The above solutions can be extended to 3D plasmas by introducing three matrices $\mathbf{T}_x$, $\mathbf{T}_y$, $\mathbf{T}_z$, one for each coordinate, all depending on the three spatial coordinates and using the total derivative D/Dt in 3D spaces,

$$\frac{D}{Dt}=\frac{\partial}{\partial t}+\mathbf{v}\cdot\nabla+[x\omega_x^2(\mathbf{r},t)\hat{x}+y\omega_y^2(\mathbf{r},t)\hat{y}+z\omega_z^2(\mathbf{r},t)\hat{z}]\cdot\nabla_{\mathbf{v}} \tag{28}$$

where $\omega_i(i=x,y,z)$ depends on all three spatial coordinates.

Accordingly, Eq. (19) generalizes into

$$f(\mathbf{X}_x,\mathbf{X}_y,\mathbf{X}_z,t)=f_0(\mathbf{T}_x^{-1}\cdot\mathbf{X}_x,\mathbf{T}_y^{-1}\cdot\mathbf{X}_y,\mathbf{T}_z^{-1}\cdot\mathbf{X}_z,t)\equiv f_0(\mathbf{T}_i^{-1}\cdot\mathbf{X}_i) \tag{29}$$

while Eq. (20) is replaced by three equations, one for each coordinate $i=x,y,z$

$$\frac{D}{Dt}\mathbf{T}_i=\begin{pmatrix}0&1\\ \omega_i^2&0\end{pmatrix}\cdot\mathbf{T}_i. \tag{30}$$

In addition, Eqs. (22) hold true separately for each coordinate.

B. 2D distributions

When the field entering the 2D Vlasov equation is directed radially and depends only on the radial coordinate r, the distribution function at time t can be represented as

$$f(\mathbf{r},\mathbf{v};t)=f_0(D\mathbf{r}-B\mathbf{v},A\mathbf{v}-C\mathbf{r}) \tag{31}$$

where A,B,C, and D are scalar functions of r and the components of the velocity parallel (v) and perpendicular ($r\dot{\theta}$) to $\mathbf{r}$ and t. These four quantities form a matrix $\mathbf{T}$. In addition, D/Dt reduces to

$$\frac{D}{Dt}=\frac{\partial}{\partial t}+v\frac{\partial}{\partial r}+\dot{\theta}\frac{\partial}{\partial\theta}+r[\omega^2(r,t)+\dot{\theta}^2]\frac{\partial}{\partial v} \tag{32}$$

where

$$\omega^2(r,t)=\Omega^2(t)\frac{2}{r^2}\int_0^r\frac{\rho(r',t)}{\rho(0,t)}r'dr' \tag{33}$$

with

$$\Omega^2(t)=\frac{e^2\rho(0,t)}{2\epsilon_0 m}. \tag{34}$$

The matrix $\mathbf{T}$ satisfies the equation of motion

$$\frac{D}{Dt}\mathbf{T}=\begin{pmatrix}0&1\\ \omega^2+\dot{\theta}^2&0\end{pmatrix}\cdot\mathbf{T}\equiv\mathbf{L}\cdot\mathbf{T}. \tag{35}$$

The introduction of the matrix $\mathbf{T}$ amounts to replacing the Vlasov equation by the partial differential system (17) or, equivalently, (20). In general, the integration of the latter system is not an easy matter and some approximate methods must be adopted, by taking into account the characteristics of MPI plasmas. To this end it is worth separating the analysis of the expansion of single charged packets under the action of some external field and its own space-charge field, from the evolution of the electron-ion plasma present in the laser focal region, which undergoes some oscillations while expanding. The first case occurs in the study of the ion cloud which leaves the laser focal region, almost free of electrons, and flies toward a detector placed at the end of a TOF spectrometer. A similar situation occurs for the most energetic electrons blasting off the laser focal region, under the action of the ponderomotive potential and the attractive potential of the ions left behind. Conversely, the less energetic electrons captured by the ion potential well undergo plasma oscillations which must be discussed in a

quite different framework.

The first group of situations is characterized by an expansion which occurs for a finite time under the action either of the self-generated space-charge field (ion packet case) or of a well-behaved ponderomotive potential and a weak ion space-charge potential. For the ions the space-charge field lasts for a time interval of the order of the time needed by a single ion with thermal velocity to span the cloud. This means that the cloud can be adequately described by restricting the velocities to the thermal range. As a consequence, we can reduce the complexity of the differential system (17) by expanding the matrix elements in power series with respect to v.

For studying the closely coupled system formed by the electrons trapped by the ion potential well, we must abandon the velocity series expansion in favor of a simple representation of the space-charge fields. Since the ion evolution is much slower than the electron oscillations, it is hard to handle the problem numerically. In this case it is important to obtain analytic formulas for the electron dynamics, which can be used for time averaging the interaction force between elecrons and ions. Then, the ion evolution can be studied by integrating the system (20) with the help of the time averaged electron contributions to the frequencies ω.

IV. VELOCITY EXPANSION

For studying the evolution of a single charged packet under the action of its own space-charge field, it proves convenient to expand A, B, C, and D in power series in the velocity. In fact, this series converges rapidly for velocities not much greater than the plasma size divided by the expansion time. This condition is usually met by the thermal velocities, so that $\mathbf{T}$ is represented by a few terms. This method will be illustrated in the following for the 1D case.

Expanding A and DA/Dt with respect to v,

$$A = A^{(0)} + A^{(1)}v + A^{(2)}v^2 + \cdots,$$
$$\frac{D}{Dt}A = \dot{A}^{(0)} + \left(\dot{A}^{(1)} + \frac{\partial}{\partial\xi}A^{(0)} + 2\xi\omega^2 A^{(2)}\right)v + \cdots + \left(\dot{A}^{(n)} + \frac{\partial}{\partial\xi}A^{(n-1)} + (n+1)\xi\omega^2 A^{(n+1)}\right)v^n + \cdots, \tag{36}$$

doing the same for B, C, and D and plugging these expansions into the system (17) we obtain

$$\begin{aligned}
\dot{A}^{(n)} &= C^{(n)} - \frac{\partial}{\partial\xi}A^{(n-1)} - (n+1)\omega^2\xi A^{(n+1)},\\
\dot{B}^{(n)} &= D^{(n)} - \frac{\partial}{\partial\xi}B^{(n-1)} - (n+1)\omega^2\xi B^{(n+1)},\\
\dot{C}^{(n)} &= \omega^2 A^{(n)} - \frac{\partial}{\partial\xi}C^{(n-1)} - (n+1)\omega^2\xi C^{(n+1)},\\
\dot{D}^{(n)} &= \omega^2 B^{(n)} - \frac{\partial}{\partial\xi}D^{(n-1)} - (n+1)\omega^2\xi D^{(n+1)},
\end{aligned} \tag{37}$$

with the initial conditions $A^{(n)}(\xi,0) = B^{(n)}(\xi,0) = C^{(n)}(\xi,0) = D^{(n)}(\xi,0) = 0$ for $n \neq 0$ and $A^{(0)}(\xi,0) = D^{(0)}(\xi,0) = 1$ and $B^{(0)}(\xi,0) = C^{(0)}(\xi,0) = 0$.

The convergence of these series will depend in general on the function ω and t. We will see that these series converge quite rapidly for $v \leq \delta/t$, δ being the effective interval in which ω is different from zero.

In an axial symetric 2D case A, B, C, and D are functions of $r, v, \dot{\theta}$, and t. Then, expanding A and DA/Dt with respect to v and $\dot{\theta}$,

$$A(r,v,\dot{\theta},t) = \sum_{mn} A^{(m,n)}(r,t)v^n\dot{\theta}^{2m},$$

$$\begin{aligned}
\frac{D}{Dt}A = {} & \dot{A}^{(0,0)} + \left(\dot{A}^{(1,0)} + \frac{\partial}{\partial r}A^{(0,0)} + 2r(\omega^2+\dot{\theta}^2)A^{(2,0)}\right)v + \cdots\\
& + \left(\dot{A}^{(n,0)} + \frac{\partial}{\partial r}A^{(n-1,0)} + (n+1)r(\omega^2+\dot{\theta}^2)A^{(n+1,0)}\right)v^n + \cdots + \dot{A}^{(0,1)}\dot{\theta}^2 + r(\omega^2+\dot{\theta}^2)A^{(1,1)}\dot{\theta}^2 + \cdots,
\end{aligned} \tag{38}$$

and doing the same for B, C, and D yields

$$\begin{aligned}
\dot{A}^{(m,n)} &= C^{(m,n)} - \frac{\partial}{\partial r}A^{(m,n-1)} - (n+1)\omega^2 rA^{(m,n+1)} - (n+1)rA^{(m-1,n+1)},\\
\dot{B}^{(m,n)} &= D^{(m,n)} - \frac{\partial}{\partial r}B^{(m,n-1)} - (n+1)\omega^2 rB^{(m,n+1)} - (n+1)rB^{(m-1,n+1)},\\
\dot{C}^{(m,n)} &= \omega^2 A^{(m,n)} - \frac{\partial}{\partial r}C^{(m,n-1)} - (n+1)\omega^2 rC^{(m,n+1)} - (n+1)rC^{(m-1,n+1)},\\
\dot{D}^{(m,n)} &= \omega^2 B^{(m,n)} - \frac{\partial}{\partial r}D^{(m,n-1)} - (n+1)\omega^2 rD^{(m,n+1)} - (n+1)\omega^2 rD^{(m-1,n+1)}.
\end{aligned} \tag{39}$$

V. EXPANSION OF SINGLE CHARGED PACKETS

For testing the method of integration based on the velocity expansion we have considered a 1D symmetric packet, initially described by the factorable distribution

$$f_0(\xi, v) = \frac{1}{\sqrt{2\pi}\sigma_v}\rho_0(\xi)\exp\left(-\frac{v^2}{2\sigma_v^2}\right) \tag{40}$$

with either a Gaussian density

$$\rho_0(\xi) = \frac{N}{\sqrt{2\pi}\sigma_0}\exp\left(-\frac{\xi^2}{2\sigma_0^2}\right) \tag{41}$$

or a spatially uniform density

$$\rho_0(\xi) = \frac{N}{\sigma_0}\mathcal{R}\left(\frac{\xi}{\sqrt{2}\sigma_0}\right) \tag{42}$$

with N the total number of particles and $\mathcal{R}(x) = 1$ for $|x| \leq 1/2$, 0 otherwise. In both cases it is worthwhile introducing the characteristic time $\tau = \sigma_0/\sigma_v$ of a particle crossing the packet with the thermal velocity σ_v. Obviously, the characteristic time τ depends on the particle mass through the thermal velocity σ_v.

In accordance with the procedure illustrated above, the system (37) has been integrated by using for ω^2 the integral (26) calculated with the density function

$$\rho(\xi, t) = \frac{1}{\sqrt{2\pi}\sigma_v}\int_{-\infty}^{\infty}\rho_0(D\xi - Bv) \times \exp\left(-\frac{(C\xi - Av)^2}{2\sigma_v^2}\right)dv. \tag{43}$$

The system (37) relative to a Gaussian distribution has been integrated for a time interval τ and a Gaussian density distribution with a number N of particles corresponding to the ratio $\mathcal{U}^{(1)}$ between the initial electric and kinetic energies,

$$\mathcal{U}^{(1)} = \frac{Ne^2\sigma_0}{\sqrt{2\pi}\epsilon_0 m\sigma_v^2} = \Omega^2(0)\tau^2 \tag{44}$$

equal to one.

Truncating the series expansion to $n = 3$ we have obtained the density $\rho(\xi, \tau)$ and the functions $A^{(0)}, B^{(0)}, C^{(0)}, D^{(0)}$ and $A^{(1)}, B^{(1)}, C^{(1)}, D^{(1)}$ plotted, respectively, in Figs. 2, 3(a), and 3(b). In particular, we have used a velocity scale of $3\sigma_v$ for the plots of Fig. 3(b). We notice that among the first-order terms, $C^{(1)}$ is the largest one and for it $C^{(1)}\sigma_v \leq 0.1$. It is, then, evident that the terms of order greater than 0 can be neglected for particles having velocities not much greater than σ_v. This conclusion refers to an expansion time of $t = \tau$ and to an initial space-charge energy equal to the kinetic one. Although the quantity τ is much smaller for electrons than for ions, one must keep in mind that the expansion lasts for a time interval equal to the detection time τ_D; in particular, for a TOF spectrometer the ratio between τ_D and the characteristic time τ is independent of the particle mass, thus allowing the use of the condition $t = \tau$ for ions as well as for electrons.

We have reiterated this procedure for a uniform distribution with a number of particles such that $\mathcal{U}^{(1)} = \Omega^2(0)\tau^2 = 3$ and an integration interval of $t = \tau/\sqrt{3}$. The relative plots are collected in Figs. 4 and 5. Also for Fig. 5(b) a velocity scale of $3\sigma_v$ has been adopted. Also for this case we found [see Fig. 5(b)] negligible the terms of order greater than zero.

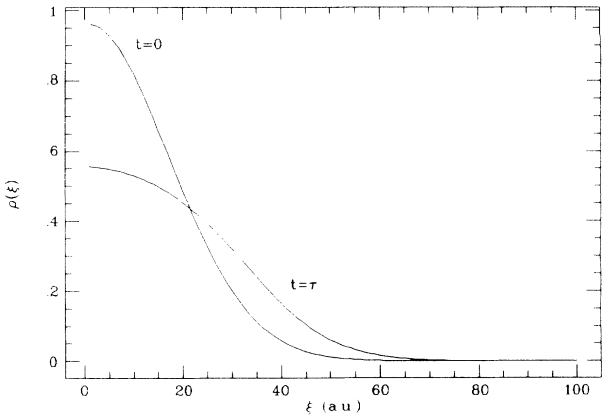

FIG. 2. Density of a 1D packet with Gaussian initial density and velocity standard deviations σ_0 and σ_v at $t = 0$ and $t = \tau = \sigma_0/\sigma_v$. The initial packet density at $\xi = 0$ was chosen in accordance with the condition $\Omega(0)\tau = 1$.

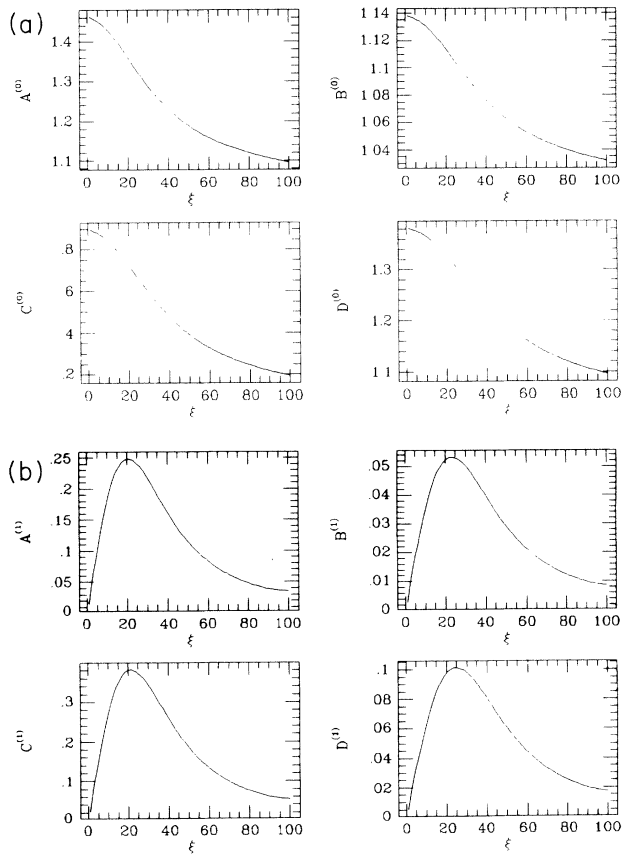

FIG. 3. Functions $A^{(0)}$, $B^{(0)}$, $C^{(0)}$, and $D^{(0)}$ [part (a)], and $A^{(1)}$, $B^{(1)}$, $C^{(1)}$, and $D^{(1)}$ [part (b)] for the Gaussian packet of Fig. 2 at $t = \tau$. A velocity scale factor of $3\sigma_v$ is assumed in the definition of the functions $A^{(1)}$, etc.

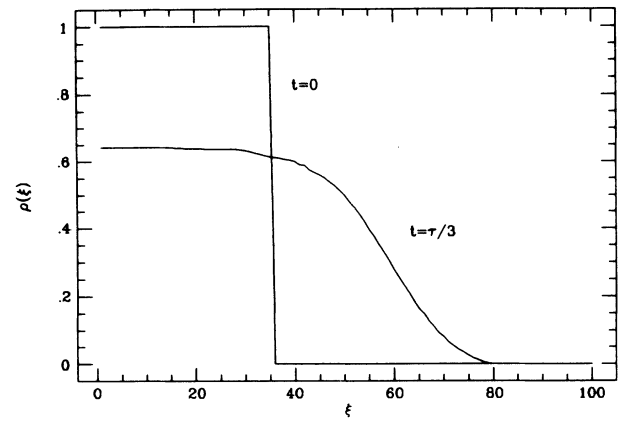

FIG. 4. Density of a 1D packet with initially uniform density in a region σ_0 and Gaussian velocity distribution with standard deviation σ_v, at $t = 0$ and $t = \tau/3 = \sigma_0/3\sigma_v$. The initial packet density was chosen in accordance with the condition $\Omega(0)\tau = 3$.

From the above two cases we draw the conclusion that $\mathbf{T}$ can be considered as velocity independent under the condition $\Omega(0)t \leq 1$. It is reasonable to expect that this conclusion holds true for other well-behaved distributions.

When we neglect the terms of the series of order greater than zero, $\mathbf{T}$ reduces to

$$\mathbf{T} = \begin{pmatrix} A^{(0)} & B^{(0)} \\ C^{(0)} & D^{(0)} \end{pmatrix} \tag{45}$$

whose equation of motion is obtained from (20) with D/Dt replaced by the partial time derivative $\partial/\partial t$.

Next, calculating the integral (43) for the Gaussian distribution gives

$$\rho(\xi, t) = \frac{N}{2\pi\sigma} \exp\left(-\frac{\xi^2}{2\sigma^2}\right), \tag{46}$$

where

$$\sigma^2(\xi, t) = B^{(0)2}(\xi, t)\sigma_v^2 + A^{(0)2}(\xi, t)\sigma_0^2. \tag{47}$$

Accordingly, the number density is represented by a Gaussian function with a standard deviation σ depending on ξ.

It is immediate to extend Eq. (46) to 2D and 3D symmetric distributions by replacing $1/2\pi\sigma$ by $1/(2\pi\sigma)^2$ and $1/(2\pi\sigma)^3$, respectively, and substituting ξ by r.

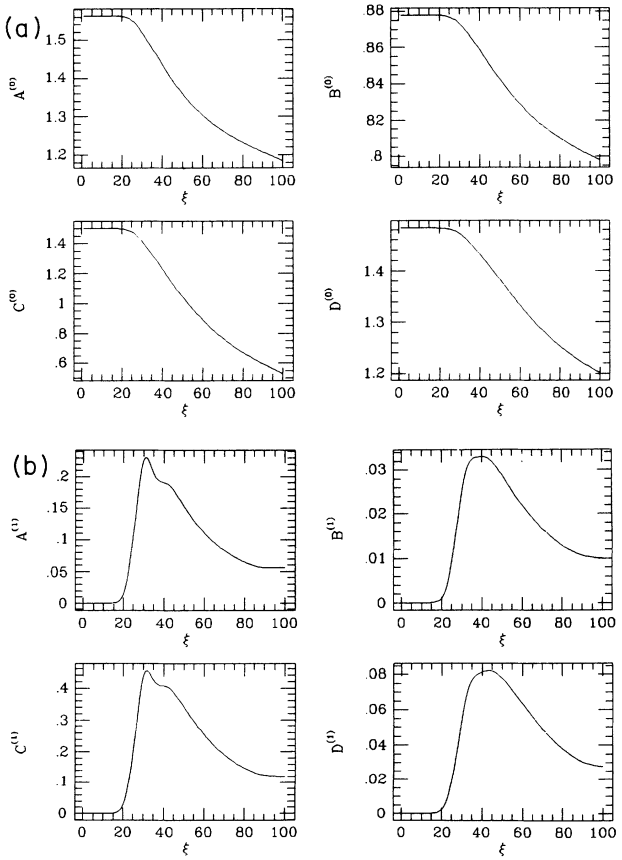

FIG. 5. Functions $A^{(0)}$, $B^{(0)}$, $C^{(0)}$, and $D^{(0)}$ [part (a)], and $A^{(1)}$, $B^{(1)}$, $C^{(1)}$, and $D^{(1)}$ [part (b)] for the uniform packet of Fig. 4 at $t = \tau = \sigma_0/3\sigma_v$. A velocity scale of $3\sigma_v$ is assumed in the definitions of the functions $A^{(1)}$, etc.

VI. LINEAR SPACE-CHARGE FIELD PROFILE APPROXIMATION

We have noticed above that in some cases $\mathbf{T}$ is approximately independent of velocity and space coordinates. Accordingly we are led to approximate Eq. (20) with an ordinary differential system in t containing an effective frequency $\Omega_{\text{eff}}^{(1)}(t)$ independent of ξ. As a consequence of this approximate representation of $\mathbf{T}$, the function $f_0(\mathbf{T}^{-1}\cdot\mathbf{X})$ satisfies only approximately the Vlasov equation with the space dependent ω, thus giving rise to an error function ϵ

$$\begin{aligned}\epsilon(\xi, v, t) &= \frac{D}{Dt} f_0(\mathbf{T}^{-1}\cdot\mathbf{X}) \\ &= \xi[\omega^2(\xi, t) - \Omega_{\text{eff}}^2] \\ &\quad \times \frac{\partial}{\partial v} f_0(D\xi - Bv, -C\xi + Av)\end{aligned} \tag{48}$$

whose quadratic integral

$$I_\epsilon = \int \epsilon^2(\xi, v, t) d\xi dv \tag{49}$$

can be used as a measure of the deviation from the exact solution. In fact, it is worthy approximating $\omega(\xi, t)$ by the function $\Omega_{\text{eff}}^{(1)}$ which minimizes I_ϵ, namely

$$\begin{aligned}\Omega_{\text{eff}}^{(1)2} &= \frac{\int \xi^2 \omega^2(\xi, t)[\partial f_0(D\xi - Bv, -C\xi + Av)/\partial v]^2 d\xi\, dv}{\int \xi^2 [\partial f_0(D\xi - Bv, -C\xi + Av)/\partial v]^2 d\xi\, dv} \\ &= \frac{\int \xi^2 \omega^2(\xi, t)\{\partial f_0[(\xi - Bw)/A, w]/\partial w\}^2 d\xi\, dw}{\int \xi^2 \{\partial f_0[(\xi - Bw)/A, w]/\partial w\}^2 d\xi\, dw} \\ &\equiv \Omega_{\text{eff}}^{(1)2}(A, B).\end{aligned} \tag{50}$$

The same considerations hold true for 2D and 3D distributions with Eq. (50) replaced, respectively, by

$$\Omega_{\rm eff}^{(2)2} = \frac{\int r\omega^2(r,t)[\mathbf{r}\cdot\nabla_{\mathbf{v}} f_0(D\mathbf{r}-B\mathbf{v},-C\mathbf{r}+A\mathbf{v})]^2 dr\,d\mathbf{v}}{\int r[\mathbf{r}\cdot\nabla_{\mathbf{v}} f_0(D\mathbf{r}-B\mathbf{v},-C\mathbf{r}+A\mathbf{v})]^2 dr\,d\mathbf{v}}$$
$$\Omega_{\rm eff}^{(3)2} = \frac{\int r^2\omega^2(r,t)[\mathbf{r}\cdot\nabla_{\mathbf{v}} f_0(D\mathbf{r}-B\mathbf{v},-C\mathbf{r}+A\mathbf{v})]^2 dr\,d\mathbf{v}}{\int r^2[\mathbf{r}\cdot\nabla_{\mathbf{v}} f_0(D\mathbf{r}-B\mathbf{v},-C\mathbf{r}+A\mathbf{v})]^2 dr d\mathbf{v}}. \tag{51}$$

Evaluating the integrals on the right-hand sides of Eqs. (50) and (51) for the 1D, 2D, and 3D Gaussian distributions and assuming that the effective frequencies $\Omega_{\rm eff}^{(1,2,3)}$ are proportional to the frequency Ω at the packet center [see Eqs. (27) and (34)],

$$\Omega_{\rm eff}^{(1,2,3)}(t) = \alpha^{(1,2,3)}\Omega^{(1,2,3)}(t) \tag{52}$$

the coefficients α^1, α^2, and α^3 are, respectively, equal to

$$\alpha^{(1)} = 0.84 \quad , \quad \alpha^{(2)} = \sqrt{\frac{2}{3}} = 0.81 \quad , \quad \alpha^{(3)} = 0.74. \tag{53}$$

Once replaced the space-charge field with that relative to an effective uniform density the equation of motion of $\mathbf{T}$ reduces to a simple differential system in t, which can be integrated by replacing ω with $\Omega_{\rm eff}(t)$.

It goes without saying that the above discussion is valid within the limits of the packet characterization in terms of its standard deviation.

VII. EXPANSION OF CHARGED PACKETS

In this section we will discuss the expansion of some typical distributions in the approximation of a linear field profile. In particular, for a 2D distribution $\Omega_{\rm eff}$ is a function of $A(t)$ and $B(t)$ [see Eq. (50)]. In view of this it is worth introducing the complex quantity $Me^{i\psi} = A + iB/\tau$, where τ is a parameter having the dimension of a time [see Sec. V]. For a Gaussian packet $\tau = \sigma_0/\sigma_v$ and, according to (47), M coincides with the ratio $\sigma(t)/\sigma_0$ between the packet size at time t and the initial one, that is M stands for the expansion ("magnification") of the packet.

With the help of M the system (22) can be recast as

$$\tau^2\frac{d^2}{dt^2}Me^{i\psi} - \Omega_{\rm eff}^2\tau^2 Me^{i\psi} = 0. \tag{54}$$

Since M and ψ take the initial values $M(0) = 1$ and $\psi(0) = 0$, as a consequence of the condition $\dot{A}(0) = 0$, $dM/dt|_{t=0} = 0$, after some algebra we obtain

$$\tau\frac{d\psi}{dt} = M^{-2}, \tag{55a}$$
$$\tau^2\frac{d^2}{dt^2}M - M^{-3} - \Omega_{\rm eff}^2(M,\psi)\tau^2 M = 0. \tag{55b}$$

A. Gaussian distributions

As a first example we will consider the evolution of a Gaussian packet with Maxwellian energy distribution. In this case, $\tau = \sigma_0/\sigma_v$ and the density will be described by a Gaussian distribution having standard deviation [see Eq. (47)]

$$\sigma^2(t) = \sigma_0^2\left(A^2(t) + B^2(t)\frac{\sigma_v^2}{\sigma_0^2}\right) \equiv \sigma_0^2 M^2(t). \tag{56}$$

In particular, for a 3D spherically symmetric Gaussian distribution

$$\Omega_{\rm eff}^{(3)2}\tau^2 = \alpha^{(3)2}\Omega^{(3)2}(t) = \alpha^{(3)2}\frac{\mathcal{U}^{(3)}}{M^3}, \tag{57}$$

where

$$\mathcal{U}^{(3)} = \frac{2Ne^2}{3(2\pi)^{3/2}\epsilon_0\sigma_0 m\sigma_v^2} \tag{58}$$

represents the ratio between the electric and thermal energies. $\mathcal{U}^{(3)}$ measures the deviation of the plasma from an ideal gas. The smaller $\mathcal{U}^{(3)}$ the more the ion cloud behaves as a rarefied gas. For typical situations $\sigma_0 \approx 10$ μm, $T \approx 300$ K, τ is of the order of 1 nsec and $\mathcal{U}^{(3)} \approx 10^{-4}$ N.

Now, introducing the above expression of $\Omega_{\rm eff}^{(3)2}\tau^2$ into (55) yields

$$M^{-1} = \frac{\cos\psi - \cos\psi_\infty}{1-\cos\psi_\infty}$$
$$\frac{t}{\tau} = \tan\frac{\psi_\infty}{2}\left[M\frac{\sin\psi}{\sin\psi_\infty} + \frac{\cos\psi_\infty}{1+\cos\psi_\infty}\ln\left(\frac{\sin[(\psi_\infty+\psi)/2]}{\sin[(\psi_\infty-\psi)/2]}\right)\right] \tag{59}$$

with $\cos\psi_\infty = \alpha^{(3)2}\mathcal{U}^{(3)}/(1+\alpha^{(3)2}\mathcal{U}^{(3)})$.

For 2D and 1D distributions $\Omega_{\rm eff}^2\tau^2$ is, respectively, equal to $\alpha^{(2)2}\mathcal{U}^{(2)}M^{-2}$ and $\alpha^{(1)2}\mathcal{U}^{(1)}M^{-1}$. Then, integrating Eq. (55) we have obtained the plots (see Fig. 6) of M vs t/τ for different values of $\mathcal{U}^{(1,2,3)}$ for 1D, 2D, and 3D distributions. For $t \gg \tau$ the expansion factor varies linearly with t, while in absence of space charge $M^2 = 1+(t/\tau)^2$.

Finally, with the help of (55a) and (57) we can show that the quantity $\int_0^\infty |\Omega_{\rm eff}^{(3)}|(t')dt'$ is less than 1.3. This result is consistent with the approximation of using functions A, B, C, and D independent of v, as remarked in Sec. V.

B. Elongated ion packets

When the ionization is produced by a fundamental mode Gaussian beam, and the process depends on a power of order p of the laser intensity, f_0 can be put in most cases in a form similar to (40) with (see Ref. [8])

$$\rho_0(\mathbf{r}) = \mathcal{N}\left\{1-\exp\left[-\frac{s}{(1+x^2/z_R^2)^p}\exp\left(-\frac{p(y^2+z^2)}{w_0^2(1+x^2/z_R^2)}\right)\right]\right\} \tag{60}$$

w_0 being the waist spot size and z_R the Rayleigh length, as illustrated schematically in Fig. 1. The saturation parameter s represents the probability of ionization at the focus of the laser beam. It can easily exceed 1 by orders of magnitude in experimental situations. $\mathcal{N}$ is the gas number density. In particular, for the ionization of Xe atoms by means of Nd:YAG laser pulses, 11 photons are needed ($p = 11$). For analyzing experiments carried out with femtosecond laser pulses, one should probably account for a more complicated spatial dependence of the ionization probability arising from resonant multiphoton ionization [12].

Due to the large value of p the factor at exponent $(1+x^2/z_R^2)^{-p}$ is different from zero only for $|x|/z_R \ll 1$, and, consequently, we can drop the term x^2/z_R^2 from the factor multiplying w_0^2 in Eq. (60). Then, expanding the exponential in power series in s, we obtain

$$\rho_0(\mathbf{r}) = \mathcal{N}\sum_{q=1}^{\infty}\frac{(-s)^q}{q!}(1+x^2/z_R^2)^{-qp}\exp\left(-q\frac{y^2+z^2}{2\sigma_0^2}\right), \tag{61}$$

where $\sigma_0^2 = w_0^2/2p$.

When s is greater than unity the ion distribution looks like a cigar with an almost uniform charge distribution on the cross section and a space-charge field directed radially and orthogonally to the cigar axis. In this case the hypothesis of linear space-charge profile is well satisfied in the directions y and z while the cloud expands freely in the x direction. Accordingly, the distribution function reads,

$$f(\mathbf{r};\mathbf{v};t) = \rho_0[(x-tv_x)\hat{x}+D\mathbf{r}-B\mathbf{v}] \times\frac{1}{(2\pi)^{3/2}\sigma_v^3}\exp\left(-\frac{v_x^2}{2\sigma_v^2}-\frac{(A\mathbf{v}-C\mathbf{r})^2}{2\sigma_v^2}\right). \tag{62}$$

In addition, averaging (62) with respect to the velocity yields

$$\rho(\mathbf{r},t) = \frac{\mathcal{N}}{(2\pi)^{1/2}\theta_x}\sum_{q=1}^{\infty}\frac{(-s)^q}{q!M_q^2}\exp\left(-\frac{r^2}{2\sigma_0^2M_q^2}\right) \times\int_{-\infty}^{\infty}dX e^{-(X-x/z_R)^2/2\theta_x^2}(1+X^2)^{-qp}, \tag{63}$$

where $\theta_x = t\sigma_v/z_R, M_q^2 = A^2+qB^2/\tau^2$, and $r = \sqrt{y^2+z^2}$.

VIII. TRANSPORT OF THE ION PACKET THROUGH A TIME-OF-FLIGHT SPECTROMETER

When the ion packet enters a TOF spectrometer the electric field is well described by the linear profile approximation of Eq. (12).

Since the packet moves through the z axis of the spectrometer it is worth replacing the time derivative with the derivative with respect to z [$d/dt = \sqrt{2e(\mathcal{E}-V_0)/m}\,d/dz$, $\mathcal{E}$ being the total particle energy in the z direction] thus writing the equation of motion of $\mathbf{T}$ in the form

$$\begin{aligned}
\frac{d}{dz}\mathbf{T}_x &= \sqrt{\frac{m}{2e(\mathcal{E}-V_0)}}\begin{pmatrix}0 & 1\\ \frac{e}{2m}V_0'' & 0\end{pmatrix}\cdot\mathbf{T}_x,\\
\frac{d}{dz}\mathbf{T}_y &= \sqrt{\frac{m}{2e(\mathcal{E}-V_0)}}\begin{pmatrix}0 & 1\\ -\Omega_y^2+\frac{e}{2m}V_0'' & 0\end{pmatrix}\cdot\mathbf{T}_y,\\
\frac{d}{dz}\mathbf{T}_z &= \sqrt{\frac{m}{2e(\mathcal{E}-V_0)}}\begin{pmatrix}0 & 1\\ -\Omega_z^2-\frac{e}{m}V_0'' & 0\end{pmatrix}\cdot\mathbf{T}_z.
\end{aligned} \tag{64}$$

In general the above system must be integrated numerically. For an electrostatic spectrometer, consisting of two diaphragms, acting as lenses, followed by a drift region, the potential V_0 along the axis is described with sufficient accuracy by the equation [13,14]

$$\begin{aligned}
V_0(z) = {} & V_1+V_2+\frac{R_1}{\pi}(E_0-E_1)+\frac{R_2}{\pi}E_1+(E_0-E_1)\frac{z-z_1}{\pi}\tan^{-1}\frac{z-z_1}{R_1}+E_1\frac{z-z_2}{\pi}\tan^{-1}\frac{z-z_2}{R_2}\\
& -\frac{z-z_1}{2}(E_0-E_1)-\frac{z-z_2}{2}E_1,
\end{aligned} \tag{65}$$

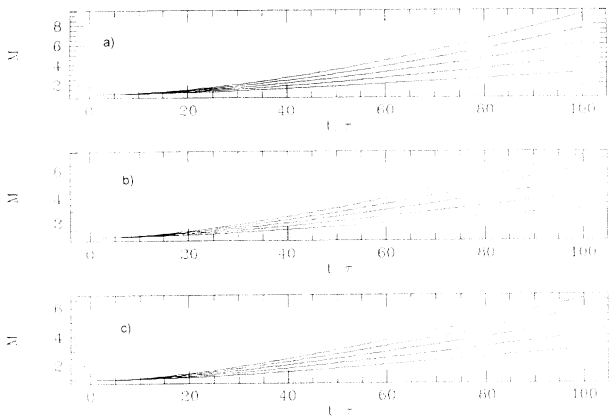

FIG. 6. Expansion factor M vs the normalized time t/τ for 1D (a), 2D (b), and 3D (c) Gaussian distributions. M was obtained by integrating Eq. (57) in the interval $0 \leq t \leq 5\tau$ ($\Omega_{\rm eff}^{(3)2}\tau^2 = \alpha^{(3)2}\mathcal{U}^{(3)}M^{-3}$, $\alpha^{(2)2}\mathcal{U}^{(2)}M^{-2}$, $\alpha^{(1)2}\mathcal{U}^{(1)}M^{-1}$ for 1D, 2D, and 3D distributions, respectively). In each case the five curves refer, respectively, to $\alpha^2\mathcal{U}$= 2, 1.5, 1, 0.5, 0 (bottom to top). The curve $\mathcal{U}$=0 corresponds to the purely thermal expansion.

where $R_{1,2}$ and $V_{1,2}$ are, respectively, the radius and the potential of the apertures located at $z = z_1, z_2$. E_0 and E_1 are the electric fields in the extraction region and in the first gap, respectively.

The ion number density relative to the MPI process produced by a Gaussian beam is described by a function similar to Eq. (63),

$$\rho(\mathbf{r},t) = \frac{\mathcal{N}\theta_x}{(2\pi)^{1/2}} \sum_{q=0}^{\infty} \frac{(-s)^q}{q!} \frac{1}{M_{qy}M_{qz}} \times \exp\left(-\frac{y^2}{2\sigma_0^2 M_{qy}^2} - \frac{z^2}{2\sigma_0^2 M_{qz}^2}\right) \times \int_{-\infty}^{\infty} dX e^{-(X-x/z_R)^2/2\theta_x^2}(1+X^2)^{-qp}, \quad (66)$$

where $M_{qy}^2 = A_y^2 + qB_y^2/\tau^2$ and $M_{qz}^2 = A_z^2 + qB_z^2/\tau^2$, while $\theta_x = B_x\sigma_v/A_x z_R$.

For integrating the system (64) we have put $\Omega_y^2 = \Omega_z^2 = e^2\rho(0;t)/\epsilon_0 m$.

We have tested the accuracy of the linear approximation by performing an experiment (described in Ref. [15]) using 30 psec 1.06 μm pulses produced in a Nd:YAG laser system. The beam was focused into a target chamber to a measured beam waist of 20 μm full width at half maximum. This corresponds to $Z_R \simeq 1$ mm. The estimated laser intensity is of the order of 10^{13}–10^{14} W/cm^2, and is typical of most nonresonant MPI experiments. The beam was focused between parallel electrodes that could be biased so as to extract ions which were measured by an electron multiplier placed at the end of a TOF spectrometer.

The waveform so obtained, was compared with the waveform obtained by integrating numerically the set of differential equations (64) and using the expansion (66). The analysis was complicated by the presence of six isotopes of xenon gas used in the experiments. The computer program circumvented this difficulty by ignoring the isotopic composition of the ion cloud when the centers of the relative distributions were separated by a distance smaller than the size of the ion cloud. Successively, different isotopes were treated separately as forming nonin-

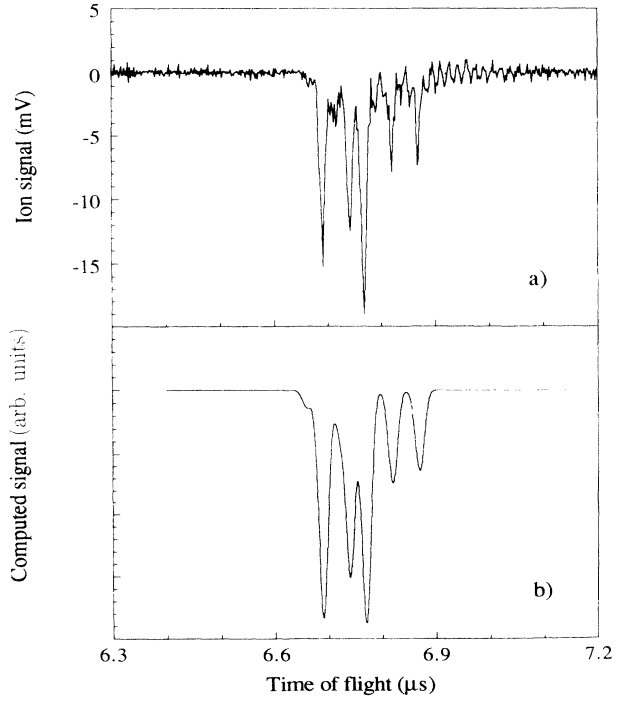

FIG. 7. Experimental ion signal (a) for a 2.3 mJ laser pulse energy and a gas pressure of 6.65 Pa, and calculated ion signal (b) for the corresponding case of N=10^3 ions.

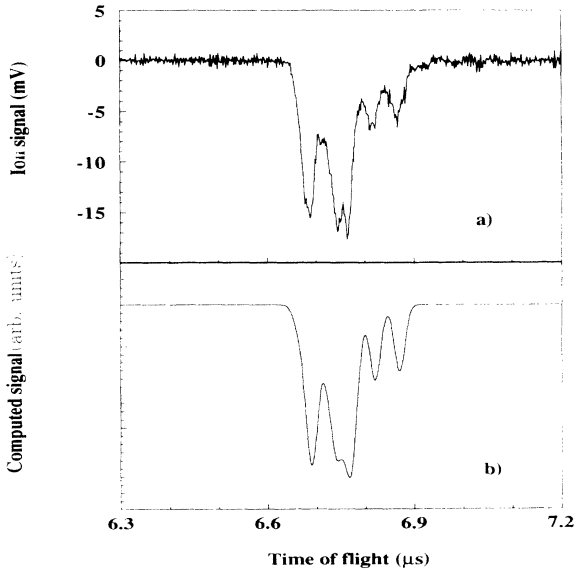

FIG. 8. Experimental ion signal (a) for a 3.2 mJ laser pulse energy and a gas pressure of 6.65 Pa, and calculated ion signal (b) for the corresponding case of N=10^5 ions.

teracting clouds. Using this procedure waveforms fitting quite well the experimental ion signals for a wide range of laser energies and number of ions were obtained. It is evident in Figs. 7(a) and 7(b), corresponding to $N = 10^3$ ions, the good agreement between the two signals for what concerns the widths of the different isotopic peaks and the height ratios which reflect the isotope natural abundancies. Figures 8(a) and 8(b) refer to the production of $\approx 10^5$ ions; it is clear that isotopic packets begin to overlap (see the two higher peaks). Figures 9(a) and 9(b) show, respectively, the experimental and theoretical waveforms in the case $N \approx 10^7$ ions. The isotopic structure of the ion signal has now completely disappeared due to the spreading and consequent overlapping of two isotopic packets. In order to elucidate how the temporal broadening of each isotopic peak varies as a function of the number of produced ions (namely, of the laser pulse intensity at fixed gas pressure), in Fig. 10 we show the ratio of the calculated full width at half maximum τ of the ^{132}Xe isotope peak to the temporal separation Δt between the centers of the ^{131}Xe and ^{132}Xe isotope packets as a function of the produced ion number N. Points below the horizontal line correspond to situations in which different isotope packets can be resolved according to the Rayleigh criterion. Thus, according to our model, a number of ions of the order of 10^5 seem to represent the critical value at which the transition between a pure ballistic regime (with independent ion packets accelerated by the extraction field) and a regime where space-charge effects cannot be neglected takes place. In terms

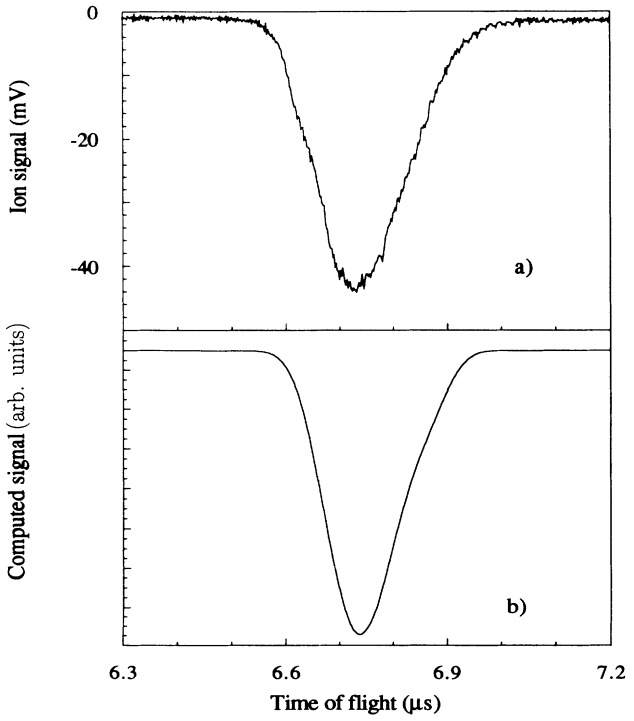

FIG. 9. Experimental ion signal (a) for a 11 mJ laser pulse energy and a gas pressure of 6.65 Pa, and calculated ion signal (b) for the corresponding case of N=10^7 ions.

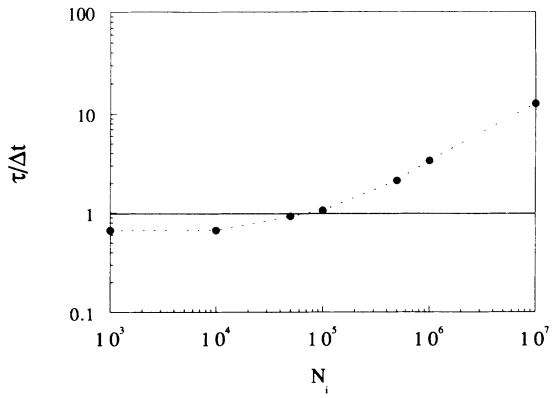

FIG. 10. Calculated ratio of the full width at half maximum τ of the ^{132}Xe isotope peak to the temporal separation Δt between the centers of the ^{131}Xe and ^{132}Xe isotope packets as a function of the produced ion number N. The value $\Delta t/\tau = 1$ (horizontal line) corresponds to the resolution limit, according to the Rayleigh criterion.

of charged particle density, the value $N = 10^5$ corresponds to $\rho = N/V \approx 10^{12}$ cm^{-3}, the interaction volume V having been determined from the laser beam parameters. The absolute number of ions produced by a single laser pulse has been estimated (within one order of magnitude) by measuring the area $\mathcal{A}$ of the experimental waveform and dividing it by the quantity eRG, where e is the electron charge, R the input resistance of the oscilloscope, and G the electron multiplier gain. These values have also been checked by exploiting measured ion yields versus laser pulse energy plots to determine the saturation condition for MPI in our experiment. More details about the experimental method can be found in Ref. [15].

IX. ELECTRON PACKET EXPANSION

In ATI experiments the velocity distribution function of the electrons is often multipeaked. These energetic particles escape rapidly from the laser focal region by leaving a partially unneutralized plasma formed prevalently of ions. In particular conditions, these unneutralized systems exhibit some very interesting plasma oscillations [5], which end up with the separation of the ions from the electrons due to the action of a generally present extraction field.

In contrast with the ions, the electron clouds are characterized by anisotropic energy distributions which deviate notably from the Maxwellian distributions assumed for the ions (see Corkum *et al.* [16]). In addition, the space-charge field depends on both ions and electrons.

When the laser pulsewidth τ_l of a Gaussian beam is much longer than b/c, with b the confocal parameter, the ponderomotive potential can be approximately represented as [see Eq. (3)]

$$V^{(\mathrm{pon})}(r,x,t) = \frac{2\pi e^2}{c\, m_e \omega^{(\mathrm{las})2}} I_0 \frac{w_0^2}{w^2(x)} \times \exp\left(-\frac{r^2}{w^2(x)}\right) \mathcal{I}(t - x/c) \qquad (67)$$

being I_0 the peak intensity and $\mathcal{I}(t-x/c)$ a function describing the pulse temporal profile.

Once an electron is ejected from the atom, it moves for some period in the laser pulse, by absorbing photons. A fraction of the absorbed photons goes to the kinetic energy of the average motion. The part that is needed for the quivering is exactly the ponderomotive potential. Many multiphoton experiments involve laser intensities in which the ponderomotive potential is comparable with the photon energy. For example at a wavelength of 1.06 μm this demands an intensity of 10^{13} W/cm^2. As a consequence of the interaction with the ponderomotive potential the energy of the electrons hitting the detector is different from the initial energy at the time in which they leave the atom. This fact may produce a shift and a broadening of the energy spectra.

In conclusion, the model we have in mind is the following: an electron distribution is produced at $t=t_0$ by multiphoton ionization inside the laser pulse. These electrons escape from the region in which they have been generated by heading through the scattering chamber. For an initial period they move in the laser pulse, while later on they proceed freely or under the influence of the space-charge field.

When the focal depth of the laser beam is much longer than the spot size, we can assume a space-charge field directed perpendicularly to the laser beam direction. In this case, with good approximation we can describe the electrons with a two-dimensional axial symmetric distribution. This holds true since in typical ATI experiments no use is made of static extraction fields.

In case we consider laser pulses sufficiently long, the electron distribution evolves under the action of a ponderomotive force directed radially. In fact, for $c\tau \gg w_0$, we can approximate $\mathbf{E}^{(\mathrm{pon})}$ by

$$\mathbf{E}^{(\mathrm{pon})} \approx -\frac{4\pi e}{c\, m_e \omega^{(\mathrm{las})2}} I_0 \frac{w_0^2}{w^2(x)} \times \exp\left(-\frac{r^2}{w^2(x)}\right) \mathcal{I}(t-x/c)\hat{r}. \tag{68}$$

Then, the distribution function relative to the electrons produced at $t=t_0$ is in general given by

$$f(\mathbf{r},\mathbf{v};t,t_0) = f_0(\, D(t,t_0)\mathbf{r} - B(t,t_0)\mathbf{v}, A(t,t_0)\mathbf{v} - C(t,t_0)\mathbf{r}, t_0), \tag{69}$$

where A, B, C, and D are described by the differential system (35) with

$$\omega^2(r,t) = \omega^{(e)2}(r,t) - \omega^{(i)2}(r,0) + \omega^{(\mathrm{pon})2}(r,t) \tag{70}$$

during the laser pulse. The ions can be considered to be at rest during the observation period due to their large mass, so that $\omega^{(i)}(t)$ has been approximated with the initial value. On the other hand, $\omega^{(\mathrm{pon})2}$ is given by

$$\omega^{(\mathrm{pon})2} = \Omega_0^{(\mathrm{pon})2} \exp\left(-\frac{r^2}{w_0^2}\right) \mathcal{I}(t), \tag{71}$$

where $\Omega_0^{(\mathrm{pon})2} = 4\pi e^2 I_0/(c m_e^2 \omega^{(\mathrm{las})2})$. For $I_0 = 10^{14}$ W/cm^2, $\lambda = 1.06$ μm and $w_0 = 10$ μm, $\Omega_0^{(\mathrm{pon})} = 0.575$ psec^{-1}. Typically, $\Omega_0^{(\mathrm{pon})}\tau$ ranges between 0.1 and 10.

A. Finite range linear profile approximation

As a first approximation we can represent $\omega^{(\mathrm{pon})2}$ as a constant different from zero in a region of radius equal to the laser spot size,

$$\omega^{(\mathrm{pon})2} = \Omega_0^{(\mathrm{pon})2} \mathcal{R}(r/2w)\mathcal{I}(t). \tag{72}$$

For this piecewise constant function ω, $\mathbf{T}$ can be represented as

$$\mathbf{T}(t,t_0) = \mathbf{T}^{(\mathrm{free})}(t,t') \cdot \mathbf{T}^{(\mathrm{pon})}(t',t_0), \tag{73}$$

where $\mathbf{T}^{(\mathrm{pon})}(t',t_0)$ is an integral of the ordinary differential system

$$\frac{d}{dt'}\mathbf{T}^{(\mathrm{pon})}(t',t_0) = \begin{pmatrix} 0 & 1 \\ \Omega_0^{(\mathrm{pon})2}\mathcal{I}(t) & 0 \end{pmatrix} \cdot \mathbf{T}^{(\mathrm{pon})}(t',t_0) \tag{74}$$

which reduces to the unit matrix for $t'=t_0$, while t' is defined by the equation,

$$|\mathbf{r} - (t-t')\mathbf{v}| = w_0 \tag{75}$$

with the additional condition $t_0 \le t' \le t$. On the other hand,

$$\mathbf{T}^{(\mathrm{pon})}(t',t_0) = \mathbf{T}^{(\mathrm{pon})-1}(t,t') \cdot \mathbf{T}^{(\mathrm{pon})}(t,t_0). \tag{76}$$

Finally, summing the contributions relative to the time interval $(0,\tau_l)$ we obtain the total distribution function f at the end of the laser pulse

$$f(\mathbf{r},\mathbf{v};\tau_l) = \int_0^{\tau_l} dt_0 f_0(\mathbf{T}^{(\mathrm{pon})-1}(\tau_l,t_0)\cdot\mathbf{X};t_0). \tag{77}$$

B. Electron energy spectrum

In most experiments the energy spectrum $\mathcal{F}(\mathbf{r}',\mathbf{v})$ is measured at large distance from the ionization region. The function $\mathcal{F}$ can be expressed as an integral over the distribution function at $t=\tau_l$,

$$\mathcal{F}(\mathbf{r}',\mathbf{v}) = \int_{\tau_l}^{\infty} dt f_0(\mathbf{T}^{(\mathrm{sc})-1}(t,\tau_l)\cdot\mathbf{X}) \tag{78}$$

where $f_0(\mathbf{r}',\mathbf{v}) = f(\mathbf{r}',\mathbf{v};\tau_l)$ while $\mathbf{T}^{(\mathrm{sc})}(t,\tau_l)$ describes the space-charge effect.

When the space-charge field is very weak, the matrix $\mathbf{T}^{(\mathrm{sc})}$ can be put in the form $\mathbf{T}^{(\mathrm{sc})} = \mathbf{T}^{(\mathrm{free})} + \delta\mathbf{T}^{(\mathrm{sc})}$, with $\delta\mathbf{T}^{(\mathrm{sc})}$ obtained by integrating perturbatively Eq. (20) at first order in ω^2,

$$\frac{d}{dt}\delta\mathbf{T}^{(\mathrm{sc})} = \begin{pmatrix} 0 & 0 \\ \omega^2[r(t)] & 0 \end{pmatrix} \cdot \mathbf{T}^{(\mathrm{free})} + \begin{pmatrix} 0 & 1 \\ 0 & 0 \end{pmatrix} \cdot \delta\mathbf{T}^{(\mathrm{sc})}, \tag{79}$$

where $r(t)$ refers to the straight electron trajectory in absence of space-charge field.

X. PARTIALLY NEUTRALIZED ION CLOUD

The plasma produced in MPI processes (ATI and RIS) is made of ions and a fraction of electrons, the more energetic electrons having left the plasma during the process of ionization or immediately after it. The remaining electrons are captured by the potential well created by the ions into a region of finite motion. Consequently, a nonneutral plasma is formed, which is characterized by intense self-electric fields.

It is known that nonneutral plasmas exhibit collective properties that are qualitativly similar to those of neutral plasmas. It has been argued in Ref. [5] that in some conditions the electron cloud remains confined for some time inside the ion potential well by undergoing some oscillations.

In Ref. [5] a fluid dynamic approach was used for studying numerically the evolution of a Gaussian distribution for both species. The large difference in the electron and ion time scales posed serious limitations to the integration algorithm used. In the following we will illustrate an analytic approach which simplifies notably the analysis of the role of the main parameters involved. In particular, we will discuss the critical dependence of the plasma dynamics on the spatial distribution and on the fraction of captured electrons.

In particular, we will see that the electron cloud undergoes breathing oscillations around its center O_e while the distance Δ between the centers O_e and O_i oscillates at the plasma frequency around a slowly increasing distance $\bar{\Delta}$. As long as $\bar{\Delta}$ is sufficiently small, the restoring force exerted by the electron cloud on the ions is able to counterbalance the force of the external extraction field. While this mechanism is active the electron packet turns out to be captured by the ion potential well. As soon as $\bar{\Delta}$ exceeds some threshold value the coupled system O_e-O_i breaks up, thus leaving the whole ion cloud free to move toward the end of the spectrometer. In conclusion, in the early phase of the plasma evolution, the electron cloud is confined inside the ion packet and exhibits high frequency breathing oscillations around its center O_e, which in turn tends to separate from O_i in virtue of the action of the extraction field, while undergoing the usual plasma oscillations. During the breathing oscillations the most energetic electrons escape from the potential well thus producing a reduction of the capture time τ_c. This complex dynamics marks the difference with the collisionless capture of electrons investigated by other authors in the contest of the propagation of solitary waves in plasmas [4, 17].

The partial neutralization of the ion cloud can modify to some extent the evolution studied in the previous section. The initial conditions are not known precisely and we are therefore restricted to making rather crude assumptions about the ion and electron distributions. In order to restrain the mathematics from getting unwieldy, we will consider Gaussian distributions for both species. These approximations should cause no concern as the most typical features of the plasma dynamics do not depend critically on the spatial distribution.

When the laser intensity is so high to produce a wealth of very energetic above-threshold ionization (ATI) electrons, most of these escape almost immediately from the potential well created by the space charge and only a small electron fraction is captured. In this situation, the plasma is unneutralized by an excess of ions and it can evolve in a way different from that observed in experiments at low intensity.

It is in fact the ion number to set the role of space-charge fields in the separation of electrons from ions under the influence of an extraction field and the expansion of the ion cloud during the flight toward the detector. Experimental evidence for this mechanism has been provided by examining resonant ionization of sodium [5c]. Due to the resonant character of the interaction, relatively low laser intensity and pulses of some nanoseconds were used.

A. Capture of the electron packet by a 2D ion potential well

Let us consider two 2D Gaussian electron and ion packets initially overlapped. We analyze the electron evolution in the linear profile approximation, as done in Ref. [5], with $\Omega^{(2)2}_{(e)\text{eff}}$ given by

$$\Omega^{(2)2}_{(e)\text{eff}}(M_e, M_i) = \Omega_0^2 \left(\frac{n_e}{M_e^2} - \frac{1}{M_i^2} \right), \tag{80}$$

where n_e represents the fraction of electrons captured by the potential well, which depends on the gas and laser intensity, while Ω_0^2 (> 0) is a constant depending on the ion density. Then, Eq. (55) specializes into

$$\tau_e^2 \frac{d^2}{dt^2} M_e + \frac{\Phi_e^2}{M_i^2} M_e - \Phi_e^2 n_e \frac{1}{M_e} - \frac{1}{M_e^3} = 0 \tag{81}$$

with $\Phi_e = \Omega_0 \tau_e$.

Due to the large mass difference, M_i changes in time much more slowly than M_e, so that M_i can be treated as a constant in the integration of the above equation.

For $M_e^{-3} + \Omega_e^2 \tau_e^2 M_e \leq 0$ the integral of Eq. (81) is a periodic function of time, defined by the integral of motion,

$$\frac{1}{2} \tau_e^2 \left(\frac{dM_e}{dt} \right)^2 + V(M_e, M_i) = E(M_i), \tag{82}$$

where $E(M_i)$ is an energy depending on time through the slowly varying quantity M_i, and $V(M_e, M_i)$ is the potential

$$V(M_e, M_i) = \frac{1}{2} \Phi_e^2 \left(\frac{M_e^2}{M_i^2} - n_e \ln M_e^2 \right) + \frac{1}{2} \frac{1}{M_e^2}. \tag{83}$$

In particular, at $t = 0$, $M_i = M_e = 1$ and $dM_e/dt = 0$, so that, $E(1) = 1 + \Phi_e^2$.

Physically, Eq. (82) indicates that the size of the electron packet undergoes anaharmonic "breathing" oscillations around the value $\bar{M}_e$ for which the potential is minimum,

$$\frac{1}{\bar{M}_e{}^2} = \frac{\sqrt{\Phi_e^4 n_e^2 + 4\Phi_e^2 M_i^{-2}} - \Phi_e^2 n_e}{2}. \tag{84}$$

Since M_i varies slowly in time, the action integral relative to Eq. (81) is a constant of motion,

$$\int_{M_{\min}}^{M_{\max}} \sqrt{E(M_i) - V(M_e, M_i)}\, dM_e = \text{const}, \tag{85}$$

$M_{\max}$ and $M_{\min}$ being two roots of the equation $E(M_i) = V(M_e, M_i)$.

For small oscillations of M_e around $\bar{M}_e$, Eq. (81) reduces to

$$\frac{d^2}{dt^2}\delta M_e + \Omega_b^{(2)2}\delta M_e = 0, \tag{86}$$

where $\delta M_e = M_e - \bar{M}_e$ and

$$\Omega_b^{(2)2} = \frac{2\Omega_0^{(2)2} n_e}{\bar{M}_e{}^2} + \frac{4}{\bar{M}_e{}^4 \tau_e^2}. \tag{87}$$

In particular, for $\Phi_e n_e M_i \gg 1$

$$\bar{M}_e \approx \sqrt{n_e} M_i, \tag{88a}$$

$$\Omega_{(e)\text{eff}}^{(2)2}(\bar{M}_e, M_i) \approx -\frac{1}{\tau_e^2 M_i^4 n_e^3}, \tag{88b}$$

$$\Omega_b^{(2)} \approx \sqrt{2}\frac{\Omega_0^{(2)}}{M_i}. \tag{88c}$$

According to (88a) the initial amplitude ΔM_e of these oscillations is equal to $\Delta M_e = |1 - \sqrt{n_e}|$. Later on, since M_i varies in time much more slowly than M_e, the amplitude of these oscillations satisfies the adiabatic law

$$\Delta M_e(t) = \Delta M_e(0)\sqrt{\frac{\Omega_b^{(2)}(0)}{\Omega_b^{(2)}(t)}} = |1 - \sqrt{n_e}|\sqrt{M_i(t)},$$

$$\frac{\Delta M_e(t)}{\bar{M}_e(t)} = \left|\frac{1}{\sqrt{n_e}} - 1\right|\frac{1}{\sqrt{M_i(t)}}, \tag{89}$$

so that the oscillations remain small during the ion expansion.

In conclusion, when the number of captured electrons does not differ notably from the ion number, as in resonant ionization processes (RIS), where the electrons have relatively small energies, the size of the electron packet oscillates slightly around that of the ion packet [see (88a)] at a frequency given by (88c).

The expansion of the ion cloud can be derived by using for $\Omega_{(i)\text{eff}}^{(2)}$ the expression

$$\Omega_{(i)\text{eff}}^{(2)2} = -\frac{m_e}{m_i}\langle\Omega_{(e)\text{eff}}^{(2)2}\rangle = \frac{m_e}{m_i}\Omega_0^{(2)2}\left(\frac{1}{M_i^2} - n_e\left\langle\frac{1}{M_e^2}\right\rangle\right), \tag{90}$$

where

$$\left\langle\frac{1}{M_e^2}\right\rangle = \frac{\int_{M_{\min}}^{M_{\max}} dM_e/(M_e^2\sqrt{E-V})}{\int_{M_{\min}}^{M_{\max}} dM_e/\sqrt{E-V}}. \tag{91}$$

In the limit of small oscillations,

$$\Omega_{(i)\text{eff}}^{(2)2} = \frac{1}{\tau_i^2 n_e^3 M_i^4}\left(1 - \frac{3}{2}n_e\Phi_e^2(1-\sqrt{n_e})^2 M_i(t)\right) \approx \frac{1}{\tau_i^2 M_i^4}. \tag{92}$$

Accordingly, when $n_e \approx 1$ the expansion rate of the ion cloud is independent of the ion density. In particular, initially the ion packet expands very slowly because the product $\Omega_{(i)\text{eff}}^{(2)}\tau_i$ is very close to 1 ($M_i \approx 1$). The presence of the electrons inside the ion packet neutralizes the repulsive forces between the ions and the nonhomogeneous plasma is temporarily stabilized.

In nonresonant ionization processes (ATI) the fraction of the captured electrons is quite small, that is $n_e \ll 1$. In this case we can neglect in (80) the electron contribution to $\Omega_{(e)\text{eff}}^{(2)2}$ (<0).

In both cases, RIS ($n_e \approx 1$) and ATI ($n_e \ll 1$) experiments, $|\Omega_{(e)\text{eff}}^{(2)}|$ is a slowly varying function of time, so that we can integrate the equation of motion of $\mathbf{T}_e$ by using the WKB approximation, thus obtaining

$$\begin{aligned}
A_e &= \sqrt{\frac{\Omega_{(e)\text{eff}}^{(2)}(0)}{\Omega_{(e)\text{eff}}^{(2)}(t)}}\cos\phi_e,\\
B_e &= \frac{1}{\sqrt{|\Omega_{(e)\text{eff}}^{(2)}(0)\Omega_{(e)\text{eff}}^{(2)}(t)|}}\sin\phi_e,\\
C_e &= -\sqrt{|\Omega_{(e)\text{eff}}^{(2)}(0)\Omega_{(e)\text{eff}}^{(2)}(t)|}\sin\phi_e,\\
D_e &= \sqrt{\frac{\Omega_{(e)\text{eff}}^{(2)}(t)}{\Omega_{(e)\text{eff}}^{(2)}(0)}}\cos\phi_e,
\end{aligned} \tag{93}$$

with $\phi_e = \int_0^t |\Omega_{(e)\text{eff}}^{(2)}(t')|dt'$.

Plugging the above expression of $\mathbf{T}$ into f_0, we obtain for the distribution function

$$\begin{aligned}
f_0(\mathbf{T}_x^{-1}\cdot\mathbf{X}_x, \mathbf{T}_y^{-1}\cdot\mathbf{X}_y) = {} & \frac{1}{(2\pi)^2\sigma_0^2\sigma_v^2}\\
& \times \exp\left[-\frac{\Phi_{(e)\text{eff}}^2 + 1}{4\sigma_0^2}\frac{\Omega_{(e)\text{eff}}^{(2)}(t)}{\Omega_{(e)\text{eff}}^{(2)}(0)}\left(r^2 - \frac{v^2}{\Omega_{(e)\text{eff}}^{(2)2}(t)}\right)\right]\\
& \times \exp\left[-\frac{1-\Phi_{(e)\text{eff}}^2}{4\sigma_0^2}\frac{\Omega_{(e)\text{eff}}^{(2)}(t)}{\Omega_{(e)\text{eff}}^{(2)}(0)}\left(x^2 - \frac{v_x^2}{\Omega_{(e)\text{eff}}^{(2)2}(t)}\right)\cos(2\phi_x)\right]\\
& \times \exp\left[-\frac{1-\Phi_{(e)\text{eff}}^2}{4\sigma_0^2}\frac{\Omega_{(e)\text{eff}}^{(2)}(t)}{\Omega_{(e)\text{eff}}^{(2)}(0)}\left(y^2 - \frac{v_y^2}{\Omega_{(e)\text{eff}}^{(2)2}(t)}\right)\cos(2\phi_y)\right]
\end{aligned} \tag{94}$$

with $\Phi_{(e)\text{eff}} = |\Omega^{(2)}_{(e)\text{eff}}(0)|\tau_e$ and $\phi_{x,y} = \arctan(\phi_e - 2\theta_{x,y})$, being $\theta_{x,y} = v_{x,y}/(x, y|\Omega^{(2)}_{(e)\text{eff}}|)$.

According to (94) a Gaussian electron packet undergoes "breathing" oscillations of steadily increasing amplitude, which vanish only for $\Phi^{(2)}_{(e)\text{eff}} = 1$. This means that the dynamics of the packet depends critically on the value of $\Phi^{(2)}_{(e)\text{eff}}$. In RIS experiments according to Eq. (88b) $\Phi^{(2)}_{(e)\text{eff}} \approx 1$, while in ATI processes $\Phi^{(2)}_{(e)\text{eff}} \gg 1$.

The oscillatory behavior of f rests on the assumption of Gaussian distribution and linear space-charge profile. In Sec. VII we have seen that Eq. (55) admits the integral of motion (82) only when Ω_{eff} depends only on M. In general, Ω_{eff} will depend on both M and ψ, as for example for a squarish distribution [see Eq. (42)]. In these cases the dynamics of the packet becomes much more complex.

B. Collision effects

In the above discussion we have neglected the collision effects. Although they are almost negligible, the breathing oscillations of the electron distribution cannot last for long. A way to include the effects of these collisions on the asymptotic behavior of f is suggested by the random field approach initially introduced by Hubbard and Thompson [17–19]. In fact, we can assimilate the collisions to the presence of a random field superimposed to the coarse grained space-charge field considered till now [see Eq. (2)]. In our case this amounts to considering an equation of motion for $\mathbf{T}$ of the form

$$\frac{d^2}{dt^2}\mathbf{T}_x + [-\Omega^{(2)2}_{(e)\text{eff}}(t) + \omega_x^{(\text{ran})2}]\mathbf{T}_x = \mathbf{0},$$
$$\frac{d^2}{dt^2}\mathbf{T}_y + [-\Omega^{(2)2}_{(e)\text{eff}}(t) + \omega_y^{(\text{ran})2}]\mathbf{T}_y = \mathbf{0}, \tag{95}$$

where $\omega_x^{(\text{ran})}$ and $\omega_y^{(\text{ran})}$ are small random quantities, mutually uncorrelated. Accordingly, the evolution of the electron packet is described by a two-dimensional randomly modulated oscillator [20].

In particular, the distribution function will read

$$f(\mathbf{X}_x, \mathbf{X}_y, t) = \langle f_0(\mathbf{T}_x^{-1}\cdot\mathbf{X}_x, \mathbf{T}_y^{-1}\cdot\mathbf{X}_y,)\rangle \tag{96}$$

where $\langle\cdots\rangle$ represents an ensemble average over $\omega_x^{(\text{ran})}, \omega_y^{(\text{ran})}$.

In case $\Omega^{(2)}_{(e)\text{eff}}(t)$ is a slowly varying function of time, the distribution function will be given by Eq. (94) with phases

$$\phi_{x,y} = \phi_e(t) + (1/2)\int_0^t [\omega_{x,y}^{(\text{ran})2}(t')/|\Omega^{(2)}_{(e)\text{eff}}|(t')]dt - \theta_{x,y}$$
$$= \phi_e + \phi_{x,y}^{(\text{ran})} - \theta_{x,y}.$$

The electron trajectories are almost periodic while $\phi_{x,y}^{(\text{ran})}$ changes very little during one period. Accordingly, $\phi_{x,y}^{(\text{ran})}$ can be treated as a Gaussian process with zero average values and variances increasing linearly in time, $\langle\phi_{x,y}^{2(\text{ran})}\rangle = t/(2\tau_r)$, τ_r being a relaxation time. τ_r will depend on the average number of collisions undergone by an electron along its trajectory, and, consequently, it will be a function of r and v.

Now, expanding (94) in Fourier series with the help of the Jacobi identity and averaging with respect to $\phi_{x,y}^{(\text{ran})}$ yields

$$f(r,v,t) = \frac{1}{(2\pi)^2\sigma_0^2\sigma_v^2}\exp\left[-\frac{\Phi^2_{(e)\text{eff}}+1}{4\sigma_0^2}\,\frac{\Omega^{(2)}_{(e)\text{eff}}(t)}{\Omega^{(2)}_{(e)\text{eff}}(0)}\left(r^2 + \frac{v^2}{\Omega^{(2)2}_{(e)\text{eff}}(t)}\right)\right]$$
$$\times\sum_{m=0}^{\infty}\epsilon_m I_m\left[\frac{\Phi^2_{(e)\text{eff}}-1}{4\sigma_0^2}\left(x^2 - \frac{v_x^2}{\Omega^{(2)2}_{(e)\text{eff}}}\right)\right]e^{-mt/\tau_r}\cos[2m(\phi_e - \theta_x)]$$
$$\times\sum_{n=0}^{\infty}\epsilon_n I_n\left[\frac{\Phi^2_{(e)\text{eff}}-1}{4\sigma_0^2}\left(y^2 - \frac{v_y^2}{\Omega^{(2)2}_{(e)\text{eff}}}\right)\right]e^{-nt/\tau_r}\cos[2n(\phi_e - \theta_y)] \tag{97}$$

with $\epsilon_n = 2$ for $n \neq 0$ and $\epsilon_0 = 1$. Accordingly, after a time of order τ_r, only the zeroth order terms survive and the oscillating part of f disappears. Physically, this corresponds to the dissipation of the breathing oscillations into thermal energy.

C. Plasma oscillations in presence of an extraction field

In accordance with the above discussion the plasma produced in resonant MPI processes has lifetime relatively long due to the partial neutralization of the space-charge fields. In this case we can use with some confidence the model discussed in Sec. II. In particular, we can imagine the plasma as formed by two clouds having centers in O_e and O_i. When a constant extraction field $E^{(\text{ext})}$ is applied along the z axis we derive from Eqs. (10) in the limit of the linear profile approximation,

$$\ddot{Z}_e - \frac{\Omega_0^2}{M_i^2}\Delta = -\frac{e}{m_e}E^{(\text{ext})}, \tag{98a}$$

$$\ddot{Z}_i + \frac{m_e}{m_i} n_e \frac{\Omega_0^2}{M_e^2}\Delta = \frac{e}{m_i} E^{(\mathrm{ext})}, \tag{98b}$$

with Ω_0 defined by Eq. (80). Next, subtracting (98a) from (98b) yields,

$$\ddot{\Delta} + \Omega_p^2 \Delta = \frac{e}{m_e} E^{(\mathrm{ext})}, \tag{99}$$

where

$$\Omega_p^2 = \Omega_0^2 \left(\frac{1}{M_i^2} + \frac{m_e}{m_i}\frac{n_e}{M_e^2} \right) \approx \frac{\Omega_0^2}{M_i^2}. \tag{100}$$

On the other hand plugging the expression (92) of $\Omega^{(2)2}_{(i)\mathrm{eff}}$ into (55b) we immediately see that the ion cloud evolves approximately as in a thermal expansion with a characteristic time $\tau_i/\sqrt{2}$,

$$M_i(t) \approx \sqrt{1+\hat{t}^2} \tag{101}$$

where $\hat{t} = \sqrt{2}t/\tau_i$.

This model can be improved by accounting for the decrease of the restoring force at large distance by introducing in Eq. (99) the function $F[r/\sigma_i(t)] = \omega^2(r,t)/\Omega_0^2$ equal to one for $r = 0$,

$$\frac{d^2}{d\hat{t}^2}\Delta + \frac{\Phi^2}{1+\hat{t}^2} F(\Delta/\sigma_0\sqrt{1+\hat{t}^2})\Delta = \frac{2e\tau_i^2}{m_e} E^{(\mathrm{ext})}, \tag{102}$$

where $\Phi = \Omega_0 \tau_i \sqrt{2}$.

For integrating the above equation we split the distance into the sum of a slowly varying part $\bar{\Delta}$ and a rapidly varying one δ_1, namely $\Delta = \bar{\Delta} + \delta_1$, with $\bar{\Delta}$ defined by

$$\frac{\Phi^2}{1+\hat{t}^2} F(\bar{\Delta}/\sigma_0\sqrt{1+\hat{t}^2})\bar{\Delta} = \frac{2e\tau_i^2}{m_e} E^{(\mathrm{ext})}. \tag{103}$$

Next, assuming $\delta_1(t)$ be so small to allow us to approximate $F(\Delta/\sigma)$ with $F(\bar{\Delta}/\sigma)$, Eq. (102) is replaced by

$$\frac{d^2}{d\hat{t}^2}\delta_1 + \frac{\Phi^2}{1+\hat{t}^2} F(\bar{\Delta}/\sigma_0\sqrt{1+\hat{t}^2})\delta_1 = -\frac{d^2}{d\hat{t}^2}\bar{\Delta}. \tag{104}$$

Since $d^2\bar{\Delta}/d\hat{t}^2 \le (2e\tau_i^2 E^{(\mathrm{ext})}/m_e)\Phi^{-2}$ and $\Phi \gg 1$, we can neglect the right side of the above equation. Consequently, within the limits of small oscillations, δ_1 satisfies the equation of motion of a slowly modulated harmonic oscillator,

$$\delta_1(t) = \delta_1(0) \frac{(1+\hat{t}^2)^{1/4}}{F^{1/4}(\bar{\Delta}/\sigma_0\sqrt{1+\hat{t}^2})} \cos[\phi(t)] \tag{105}$$

with $\phi = \Phi \int^{\hat{t}} \frac{F^{1/2}}{\sqrt{1+\hat{t}^2}} d\hat{t}$.

For 2D Gaussian distributions the function F reads,

$$F\left(\frac{r}{\sigma}\right) = \frac{1-e^{-r^2/2\sigma^2}}{r^2/2\sigma^2} \approx \frac{1}{1+r^2/2\sigma^2}. \tag{106}$$

Consequently,

$$\bar{\Delta} = \Delta_{\max}\left(1 - \sqrt{1 - \frac{2\sigma_0^2}{\Delta_{\max}^2}(1+\hat{t}^2)}\right), \tag{107}$$

where

$$\frac{\Delta_{\max}}{\sigma_0} = \frac{m_e \sigma_0 \Omega_0^2}{eE^{(\mathrm{ext})}} = \frac{\sigma_0 l \rho_i(0)}{4\epsilon_0 E^{(\mathrm{ext})}} = 10^8 \frac{N}{2\pi l \sigma_0 E^{\mathrm{ext}}}. \tag{108}$$

Here $\rho_i(0)$ represents the volume number density of the ions on the axis of the 2D distribution, l stands for the effective dimension of the plasma along the axis while N is the total number of ions. For typical conditions ($\sigma_0 \approx 10$ μm, $l = 1$ mm),

$$\frac{\Delta_{\max}}{\sigma_0} \approx 5 \times 10^{-3} \frac{N}{E^{(\mathrm{ext})}} \tag{109}$$

for a field measured in V/cm.

The system electron-ion will be bound for a time of the order of

$$t_{\max} = \sqrt{2}\tau_i \sqrt{\frac{\Delta_{\max}^2}{\sigma_0^2} - 1}. \tag{110}$$

In addition, it follows from (107)

$$\delta_1(0) < \bar{\Delta}(0) \approx \Delta_{\max}\left(1 - \sqrt{1 - \frac{2\sigma_0^2}{\Delta_{\max}^2}}\right) \approx \frac{\sigma_0^2}{\Delta_{\max}} \tag{111}$$

while combining (105) with (107) yields, for $\Delta_{\max}/\sigma_0 \gg 1$:

$$\frac{|\delta_1(t)|}{\sigma(t)} < \frac{1}{2}\left(\frac{\sigma_0}{\Delta_{\max}}\right)^{1/2} \frac{1}{(1+\hat{t}^2)^{1/2}} \times \left(1 - \sqrt{1 - \frac{2\sigma_0^2}{\Delta_{\max}^2}(1+\hat{t}^2)}\right)^{1/4}. \tag{112}$$

Consequently, the amplitude of the oscillation of $\delta_1(t)/\sigma(t)$ decreases from the initial value $\sigma_0/\Delta_{\max}$ to $(\sigma_0/\Delta_{\max})^{3/2}$. Then, the initial assumption of small oscillation is well satisfied for $\Delta_{\max} \gg \sigma_0$.

XI. CONCLUSIONS

In this paper we have analyzed the plasma produced in MPI processes (ATI and RIS) by dwelling on the dynamics of the ions and the electrons. We have shown that in most experimental conditions the integral of the Vlasov-Maxwell equation is represented by the initial distribution function with arguments transformed by a time-dependent matrix **T**. In other words, the plasma evolution is represented by a transformation **T** acting upon the coordinates **r**-**v** of the particle phase space. Hence,

the integration of the Vlasov-Maxwell equation reduces to the integration of the equation of motion of the matrix **T**, which depends on the external field present in the scattering chamber and in the spectrometer, and on the densities of the ion and electron packets. Combining the equation of motion of **T** with the electron and ion densities, a closed system of equations is obtained.

In most cases the collision effects are so small that they can be accounted for by introducing a random field, so that the distribution function is given by an ensemble average over such a random field. In practice such a random field correponds to a random phase contribution to the matrix **T**, which can be treated as a Gaussian process.

In concluding this paper, it is worth pointing out some approximations and limits of the analysis we have developed in order to put our approach in perspective in the more general field of numerical models put forward to analyze the plasma behavior in different physical conditions.

In particular, the main aim of our model was to investigate the dynamics of charged packets produced in MPI experiments, with special attention paid to the case of nonresonance MPI where most of the electrons are produced as energetic ATI electrons, thus readily leaving the interaction volume, while the thermal ions evolve under the action of their own space-charge field and of an extraction static field. In the hypothesis of a linear space-charge field profile and disregarding the interaction between ion and electron clouds, our analysis has been used for interpreting the temporal broadening of ion peaks observed at the output of a TOF spectrometer, as well as the change in their relative temporal positions observed in actual well-controlled experimental conditions.

This evolution of ion packets during the passage through an electrostatic time of flight can be studied by integrating a differential system, thus simplifying the evaluation of experimental results and assisting in planning experiments.

We have carried out our calculation only in the case of two-dimensional plasmas, and the extension of the model to more general and complete three-dimensional situations is not straightforward, although we are presently making an effort in this direction. Moreover, we have made rather crude assumptions about ion and electron distributions, in order to restrain the mathematics from getting unwieldy. We have, thus, been restricted to use *well-behaved* (Gaussian) distributions for both charged species. This, obviously, prevents the analysis of plasma oscillations in a more general context. For instance, the effect of Landau damping on the evolution of plasma oscillations cannot be handled by the simple expansion in powers of v used by us [see Eq. (36) and following]. This limit of our model in its present form represents a serious warrant to future studies of more general situations.

In spite of the above limits, the analysis based on distribution functions appears more flexible and complete than that based on the fluid model. The kinetic theory can accommodate deviations of the space-charge field profile from the linear one. Finally, analytic solutions can be worked out in several significant cases. On the opposite, the fluid model developed in Ref. [5] can be used only for Gaussian packets with Maxwellian energy distributions and in absence of collisions.

The advantages of the kinetic approach become more evident in the study of the interaction of electrons and ions, where the limits of some fluidynamic models based on Gaussian spatial distributions become more severe.

[1] L. A. Lompré, A. L'Huillier, G. Mainfray, and C. Manus, J. Opt. Soc. Am. **B2**, 1906 (1985); S. L. Chin and N. R. Isenor, Can. J. Phys. **48**, 1445 (1970); P. Agostini, G. Barjot, G. Mainfray, C. Manus, and J. Thebault, IEEE J. Quantum Electron. **QE-6**, 782 (1970); M. Cervenan and N. R. Isenor, Opt. Commun. **13**, 175 (1975).

[2] A. L'Huillier, X. F. Li, and L. A. Lompre, J. Opt. Soc. Am. **B7**, 527 (1990).

[3] N. A. Krall and A. W. Trivelpiece, *Principles of Plasma Physics* (McGraw-Hill, New York, 1973).

[4] R. C. Davidson, *Theory of Nonneutral Plasmas* (Benjamin, Reading, 1974).

[5] (a) F. Giammanco, Phys. Rev. A **36**, 5658 (1987), Phys. Rev. A **40**, 5171 (1989); (b) F. Giammanco, Phys. Rev. A **40**, 5160 (1989); (c) F. Giammanco, G. Arena, R. Bruzzese, and N. Spinelli, Phys. Rev. A **41**, 2144 (1990).

[6] J. M. Dawson, Phys. Fluids **5**, 445 (1962); Rev. Mod. Phys. **55**, 403 (1983).

[7] C. K. Birdsall and A. B. Langdon, *Plasma Physics via Computer* (McGraw-Hill, New York, 1985).

[8] M. R. Sogard, J. Opt. Soc. Am. **B5**, 1890 (1988); see also, G.S. Voronov and N. B. Delone, Zh. Eksp. Teor. Fiz. **50**, 78 (1966) [Sov. Phys. JETP **23**, 54 (1966)]; P. Agostini, G. Barjot, G. Mainfray, C. Manus, and J. Thebault, IEEE J. Quantum Electron. **QE-6**, 782 (1970).

[9] L. Jonsson, J. Opt. Soc. Am. B **4**, 1422 (1987); see also, T. W. B. Kibble, Phys. Rev. Lett. **16**, 1054 (1966); P. Luchini, C. H. Papas, and S. Solimeno, Appl. Phys. B 28 (1982); P. Luchini and S. Solimeno, Phys. Lett. **91A**, 438 (1982).

[10] P. Kruit and F. H. Read, J. Phys. E **16**, 313 (1983).

[11] S. Jackson, *Classical Electrodynamics* (Wiley, New York 1960).

[12] R. R. Freeman, P. H. Bucksbaum, H. Hilchberg, S. Darak, D. Schumaker, and M. Geusic, Phys. Rev. Lett. **59**, 1092 (1987); P. Agostini, A. Antonetti, P. Berger, M. Crance, A. Migus, H. G. Muller, and G. Petite, J. Phys. B **22**, 1971 (1989); X. Tang, A. Lyras, and P. Lambropoulos, Phys. Rev. Lett. **63**, 972 (1989).

[13] K. R. Spangberg, *Vacuum Tubes* (McGraw-Hill, New York, 1948).

[14] D. W. Heddle, *Electrostatic Lens Systems* (Hilger, Bristol, 1991); D. A. Dahl, numerical code SIMION, Idaho National Engineering Laboratory.

[15] C. de Lisio, C. Altucci, R. Bruzzese, T. Di Palma, S. Solimeno, N. Spinelli, and V. Tosa, J. Phys. B **25**, 4781 (1992).

[16] P.B. Corkum, N.H. Burnett, and F. Brunel, Phys. Rev. Lett. **62**, 1259 (1989).

[17] S. Ichimaru, *Basic Principles of Plasma Physics: A Sta-*

tistical Approach (Benjamin, Reading, 1973).
[18] W. B. Thompson and J. Hubbard, Rev. Mod. Phys. **32**, 714 (1960).
[19] W. B. Thompson, *An Introduction to Plasma Physics* (Addison-Wesley, Reading, MA, 1964).
[20] B. Crosignani, P. Di Porto, and S. Solimeno, Phys. Rev. **186**, 1342 (1969); B. Crosignani, P. Di Porto, and S. Solimeno, Phys. Rev. D **3**, 1729 (1971); B. Crosignani, P. Di Porto, and S. Solimeno, Phys. Rev. Lett. **26**, 1130 (1971).